An Evaluation of Optical Fiber Strain Sensing for Engineering Applications

Douglas Alan Harold

Thesis submitted to the faculty of the Virginia Polytechnic Institute and State University
in partial fulfillment of the requirements for the degree of

Master of Science
In
Engineering Mechanics

John C. Duke, Jr.
Luther G. Kraige
Ronald D. Kriz

February 16, 2012
Blacksburg, Virginia

Keywords: Fiber Bragg grating, Distributed strain sensing, Strain transfer, Optical fiber strain sensor, Durability

An Evaluation of Optical Fiber Strain Sensing for Engineering Applications

Douglas Alan Harold

ABSTRACT

A fatigue test has been performed on 7075-T651 aluminum specimens which were bonded with polyimide coated optical fibers with discrete Bragg gratings. These fibers were bonded with AE-10 strain gage adhesive. The results indicate that lower strain amplitudes do not produce cause for concern, but that larger strain amplitudes (on the order of 3500 με) may cause some sensors to become unreliable.

The strain response of acrylate coated optical fiber strain sensors bonded to aluminum specimens with AE-10 and M-Bond 200 strain gage adhesives was investigated with both axial and cantilever beam tests. These results were compared to both the strain response of conventional strain gages and to model predictions. The results indicate that only about 82.6% of the strain in the specimen was transferred through the glue line and fiber coating into the fiber. Thus, multiplying by a strain transfer factor of approximately 1.21 was sufficient to correct the optical fiber strain output. This effect was found to be independent of the adhesive used and independent of the three-dimensional profile of the glue line used to attach the fiber. Finally, this effect did not depend on whether the fiber had a polyimide or an acrylate coating.

Further investigation was conducted on the feasibility of using optical fiber strain sensors for monitoring subcritical damage (such as matrix cracks) in fiber reinforced composite materials. These results indicate that an array of optical fibers which monitor the strain profile on both sides of a composite panel may be sufficient for these purposes.

Acknowledgements

I would like to thank those who served on my advisory committee, and who have mentored me in my graduate studies: Dr. Glenn Kraige, Dr. Ron Kriz, and especially my advisor Dr. John Duke. I have appreciated our many long and wide-ranging discussions.

I would like to thank The American Society for Nondestructive Testing (ASNT) for a generous fellowship grant which made much of this research possible, and Luna Technologies for their interest in promoting education and research and for the use of their instrumentation, software, and technical assistance. Work preliminary to this research was funded by the National Aeronautics and Space Administration (NASA). The support by these organizations is greatly appreciated.

Finally, I would like to express my gratitude for the support of my friends, my family, and especially my wife, Lindsay, who is my best friend, companion, and greatest supporter. I would like to dedicate this to her, to our daughter, and to our Creator and Savior.

Table of Contents

List of Figures

List of Tables

List of Abbreviations

AE-10	M-Bond AE-10 Strain Gage Adhesive
AE-15	M-Bond AE-15 Strain Gage Adhesive
cRIO	CompactRIO 9014 National Instruments data acquisition system
DSS	Distributed Sensing System
FBG	Fiber Bragg Grating
HSDSS	High Speed Distributed Sensing System

Chapter 1

Introduction

In recent years, optical fibers have been increasingly used for remote sensing in place of conventional electrical sensors. In theory, these optical fiber sensors may be configured to measure many different parameters (even many different parameters along the length of a single optical fiber). In each case, a specialized transducer is employed which converts the measurand of interest into axial strain in the fiber. In the most basic configuration, the sensing fiber is simply bonded (with conventional strain gage adhesive) directly to a structural member and used as a strain sensor, or it may be embedded in a composite, being placed in between plies during fabrication (without additional adhesive).

There are now several different types of optical fiber sensors and several different methods for interrogating them (Erdogan, 1997; Kersey, 1996; Peairs, 2009). Initially, it was quite common for fiber optic sensors to utilize discrete Bragg gratings written into the core of the fiber (Hill, 1997; Kersey, 1997), and a common design employed gratings which were each about 5 mm long placed on regular intervals along the length of the fiber (typically 10 mm center to center). These early designs often employed data acquisition and post-processing which returned a single strain value for each Bragg grating. Other approaches to optical fiber sensing have also been developed which do not require discrete Bragg gratings (Guemes, 2010). Instead, it is now possible to gain strain information from multiple points within a single long Bragg grating or from an optical fiber which has no Bragg grating at all (Gifford, 2011; Guemes, 2010). These techniques also improve spatial resolution greatly. Whereas, the early designs which return a single strain value for each Bragg grating produce a spatial resolution equal to that of the distance between gratings along the fiber (typically 10 mm), these newer techniques produce

theoretical spatial resolutions as low about a tenth of a millimeter. Thus, one may improve the signal quality by averaging and reducing the data by a factor of 10, and still retain a spatial resolution of around 1 mm without reducing time resolution.

Further improvement may be obtained by smoothing the data using a moving average without significant loss of information. One must remember that the output for this type of system is a 2D matrix of strain data with one dimension corresponding to time (i.e. each row gives the strain distribution in the fiber for a particular instant in time) and the other dimension of the strain matrix corresponding to length along the fiber (i.e. each column gives the strain as a time series for a particular point in the fiber). In this context, one may smooth the data by performing an unweighted five point moving average on each row (i.e. for each instant in time), and thereby improve the signal without reducing frequency content or losing time resolution. In fact, some studies show that the adhesive and fiber coating require on the order of a few millimeters to fully transmit step-like changes in strain into the fiber core anyway (Betz, 2003). Therefore, this moving average (in the space dimension) may be quite appropriate considering the strain transfer capabilities of the adhesive and fiber coating.

The distributed sensing capabilities of optical fiber strain sensing offer many advantages over conventional strain gages. However, they also introduce a need for additional testing. For instance, with optical fiber coated in either acrylate or polyimide and bonded with conventional strain gage adhesive for strain sensing, one finds that the strain induced in the fiber is not typically equal in magnitude to that known to exist in the specimen to which it is bonded (Habel, 2007).

In theory, this effect is due to the elastic nature of both the adhesive used for attachment and the protective coating of the fiber itself. Both of these layers lie between the glass of the optical fiber (where strain measurements are made) and the engineering structure to which it is bonded and which applies the strain to be measured. Since these layers are not rigid, they are incapable of transferring 100% of the strain present in the structure into the core of the fiber. Thus, a multiplication factor (or strain transfer factor) is needed to convert the measured strain into actual “true” strain present in the structure (Li, 2005; Zhou, 2006). This is consistent with finite element modeling of the strain transfer properties of various fiber optic coatings (Betz, 2003). With this in mind, one might expect that different adhesive and coating combinations (including

both composition and thickness) should yield different strain transfer capabilities and thus different multiplication factors.

This does not necessarily represent a significant problem if one is able to accurately determine a factor (analogous to the gage factor for a conventional strain gage) which converts the measured strain to the actual strain. However, once one determines this factor, it is necessary to determine through additional testing whether this strain transfer factor is consistent. In other words, it is necessary to determine the set of conditions under which one may rely on the strain transfer to behave as expected, and to determine those conditions which may cause the strain transfer to become unpredictable. Additionally, as noted by Habel (2007), the fiber attachment procedures need to be standardized according to good operating practices in order to ensure that a consistent and predictable strain transfer is obtained and to ensure that the glue line is both durable and reliable.

Furthermore, it is necessary to ensure that the strain transfer is linear, such that the strain transfer factor is constant and does not change with the magnitude of strain applied, and in so doing, it is necessary to show that this factor is the same in compression as it is in tension. In addition, there are several other important questions which must be answered. As mentioned earlier, will different adhesives transfer strain differently? Does the strain transfer capability of a glue line depend on the cross-sectional profile of the glue line or on the details of the cure cycle used? Will the strain transfer change with age or fatigue? What conditions are capable of altering the strain transfer factor, and thereby potentially making the sensing system unreliable? Finally, how does one accurately determine the correct strain transfer factor for an engineering component in service, and does it depend on the material to which the sensor is bonded, or on the coating of the optical fiber?

Experimentally, the strain transfer issue may be investigated using an axial specimen with an optical fiber bonded to measure axial strain, or by using the same specimen loaded in as a cantilever beam. However, there are several advantages in using a cantilever beam test instead of an axial test performed with a mechanical load frame for investigating this strain transfer issue. First, it is much easier to ensure that the specimen is not exposed to any additional (unintentional) loading. For instance, any slight misalignment in the hydraulic grips of the load frame will introduce an unintended (and unknown) moment to the end conditions of the loaded

specimen which will cause a strain gradient along the specimen - thus making strain transfer determination more problematic. Second, an axial test (with slightly misaligned grips) requires that the locations of strain gages (with respect to locations within the optical fiber glue line) be accurately determined before one can compare the results of an optical fiber system with those of conventional strain gages. However, this is not necessary for a cantilever beam test in which only the strain gradient need be determined with both systems. In other words, the strain transfer issue may be investigated via a cantilever beam test by simply comparing the strain gradient measured by optical fiber sensors with that measured by a series of conventional strain gages without regard to the positioning of one set of sensors with respect to that of the other.

In addition to these reliability and strain transfer concerns, and in order to take full advantage of the spatial resolution capabilities of optical fiber strain sensing, it is necessary to determine whether or not the distributed sensing capabilities of this technology make it possible to detect the presence or formation of subcritical, embedded damage in composite materials. A common example of this sort of subcritical damage in composites is a typical matrix crack (see Figure 1.1).

In theory, the strain field near a matrix crack in a composite material should include a gradual increase in strain (i.e. a strain gradient) as one approaches the crack from one side and then a similar decrease in strain as one departs from the crack location on the other side. This is because the crack itself does not carry a load. However, since the matrix crack is an embedded flaw

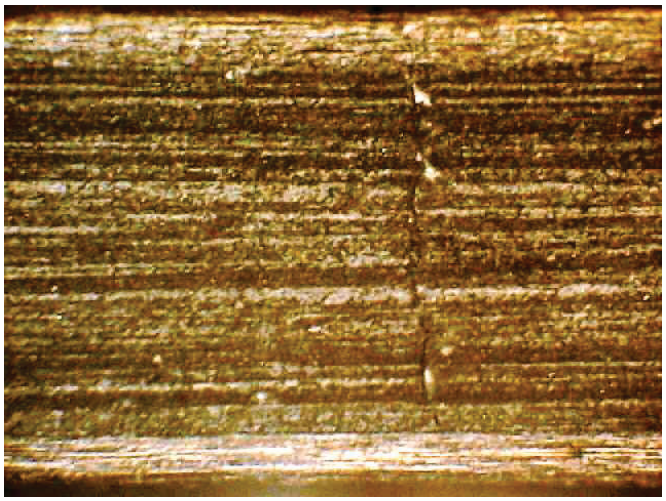

Figure 1.1 Matrix crack through the interior plies of a $[0, 90_3]_S$ fiber-reinforced graphite-epoxy composite specimen.

which does not traverse completely through the material from one side to the other, there remains an intact portion of the cross-section (typically consisting predominantly of reinforcement fibers) which carry the full load in that cross-section. On each side of the crack, this load is gradually transferred from those intact fibers (which span the matrix crack) into the layers which contain the crack. This produces a characteristic strain gradient on each side of the crack itself. Therefore, if one knows certain material properties of a composite material, it may be possible to not only detect the presence of embedded, subcritical damage (such as matrix cracks), but also predict the severity of those flaws with surface or embedded optical fiber sensing.

The purpose of this project was to investigate these durability and strain transfer issues, and the usefulness of optical fiber sensing for detecting subcritical damage in fiber reinforced composite materials. Thus, several mechanical tests were performed using multiple strain gage adhesives with multiple glue line profiles and both aluminum and composite specimens. These tests included both cantilever beam deflection and axial loading in both tension and compression. The optical fiber strain measurements resulting from these tests were compared to the strain measurements taken simultaneously from adjacent conventional strain gages, and to the strain calculated from load cell measurements using the appropriate constitutive relationships.

The following chapters are intended to present the various areas of research undertaken in this Master's thesis project. These particular areas were chosen because they seemed sufficient to evaluate the capability of optical fiber sensors and their suitability for structural health monitoring applications. Although these chapters are standalone documents which describe separate research projects, it is hoped that the reader recognizes that taken together they demonstrate a method for characterizing the dependability and usefulness of optical fiber sensors.

A more detailed description of the approach taken in this project is as follows:

Chapter 2: A Durability Assessment of Optical Fiber Bragg Grating Strain Sensors

In this chapter, the durability of polyimide coated optical fibers with discrete Bragg grating strain sensors is discussed. These durability issues concern not only the fiber sensors themselves, but the stability of the glue line as well. The attachment of optical fiber strain sensors involves a series of materials and interfaces, including the adhesive and the fiber coating (both polymers), as well as the fiber cladding and the fiber core (both optical fiber glass). Since the durability of the glass of optical fiber has been tested many times, this investigation focused on the durability of glue line itself, and its ability to reliably transfer strain into the fiber.

Chapter 3: The Effects of Adhesive Geometry and Type on Strain Transfer for Optical Fiber Strain Sensing

Since strain gage adhesives and fiber coatings are not rigid materials, it should not be expected that they will be capable of transferring strain into an optical fiber perfectly. Instead, it turns out that only a portion of the applied strain will be detectable in the fiber core. This chapter deals with determining the fraction of strain that is transferred into the fiber, and investigating whether or not the type of strain gage adhesive or three-dimensional geometry of the glue line has any effect on this factor.

Chapter 4: Optical Fiber Sensing for Damage Detection in Composites

While earlier chapters dealt with the dependability and reliability of optical fiber strain sensing, this chapter investigates the applicability of these sensors for certain structural health monitoring applications. In particular, a proof of concept test is discussed in which optical fiber strain sensing was used to determine the strain profile along both surfaces of a fiber reinforced composite specimen in tension. The strain profiles along both surfaces of such a material may be used together to predict the formation of subcritical damage, and to monitor its progression.

Chapter 2

A Durability Assessment of Optical Fiber Bragg Grating Strain Sensors

Abstract

A mechanical test has been performed on 7075-T651 aluminum specimens that were bonded with optical fiber strain sensors produced by Luna Innovations, Inc. These sensors were fiber Bragg gratings (FBG's) that were written into the fiber core at the time the fiber was manufactured. The purpose of the test was to characterize the durability of the fibers, sensors, adhesive bond, etc. under mechanical fatigue loading. A Distributed Sensing System (DSS), Version 1.X (part number OBR - 80 NF), provided by Luna Innovations was used to interrogate the gratings. The results of this test are somewhat mixed with lower strain amplitudes (3000 με) not producing cause for concern, and larger strain amplitudes (3500 με) producing some cause for concern in a select few FBG sensors.

2.1 Introduction

The many advantages of optical fiber sensors over conventional technology are well known and have been discussed often in recent years. However, as with any relatively new technology, it is necessary to establish lifetime performance characteristics, especially when the technology is to be deployed in remote or otherwise inaccessible locations. In fact, it is often the advantages of fiber optic sensors that make them so well-suited for just this type of application. There are, of course, many different types of testing regimes that need to be explored, but this study focused primarily on mechanical fatigue testing at room temperature. Needless to say, optical fiber has been fatigue tested many years ago; however, very little has been done to assess the durability of fiber and fiber Bragg gratings (FBG's) bonded to metallic specimens using conventional strain

gage adhesive. Therefore, the purpose of this study was to characterize the durability of optical fiber strain sensors when bonded to aluminum with common strain gage adhesive and exposed to mechanical fatigue at room temperature.

2.2 Testing Methods

All of the data discussed in this report were obtained using a Distributed Sensing System (DSS) Version 1.X (part number OBR - 80 NF, serial number 05017032). The system was operated with DSS Software Version 2.1, which was set up to scan over a range of 41.54 nm and collect data using a gain of 20dB. The system was set to scan and log data as rapidly as possible; given these parameters, the scan rate turned out to be less than 0.25 Hz. The strain sensors used in these tests were fiber Bragg gratings written into the core of single-mode optical fiber at the draw tower before the application of a polyimide coating. These gratings had a nominal Bragg wavelength of 1546 nm. The DSS 1.X, the software and the strain sensors were all provided by Luna Innovations, Inc. (Blacksburg, VA).

The strain gage adhesive used in this test for bonding of the optical fiber was AE-10 (a two part epoxy) purchased from Vishay Micro-Measurements (Control Number 0653). The surface preparation technique and the mixing of epoxy followed Vishay Instruction Bulletin B-137 very closely. Of course, the fiber application technique needed to be modified from that described in B-137 which was designed for conventional strain gages. Once the surface preparation was completed, the optical fibers were positioned in the desired location and held with transparent tape placed approximately 0.125 inch from each end of the desired bond line. Next the epoxy was mixed according to the instructions and applied using a 22 gauge syringe (which had been blunted to avoid damaging the fiber).

The fiber assembly was manufactured according to the design in Figure 2.1. This design utilizes a flexible protective sleeve extending from the splice to the testing region of the fiber; the end of this tubing was also bonded to the specimen with AE-10 adhesive in order to protect the ingress of the fiber.

Mechanical testing of the strain gage assembly was accomplished with two specimens manufactured from 38.1 mm wide by 12.7 mm thick (1.5 in wide by 0.5 in thick) 7075-T651 aluminum flat bar, see Figures 2.2 and 2.3. The coefficient of thermal expansion for this material

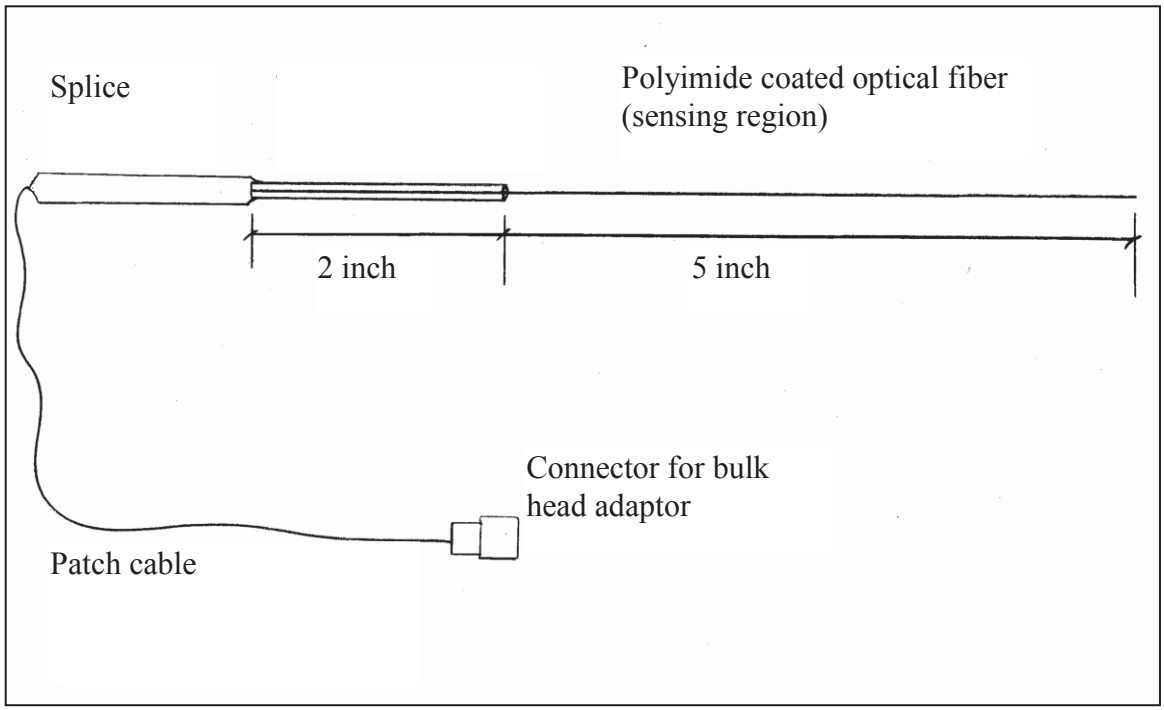

Figure 2.1 Optical fiber assembly.

is 13.1 με/^{o}F, and the elastic modulus is 71.7 GPa (10,400 ksi). The overall specimen length was 270 mm (10.625 in) for each. However, a 114.3 mm (4.5 in) long test section was milled into the central portion. This test section was 12.7 mm by 12.7 mm (0.5 in by 0.5 in) square in cross-section. Thus, these specimens had the shape of a square dog bone.

Both specimens were tested by axial loading using a hydraulic Instron Mechanical Test Stand (MTS). The fatigue test was performed at a cycle rate of 10 Hz with the nominal amplitudes given in Table 2.1 around a mean strain of zero. Actually, the test was performed in "load control" mode, because this provided the most dynamic stability. However, the load amplitudes were chosen to produce the strain levels indicated.

Table 2.1 Fatigue Test Design

Specimen	Sensors Monitored	Maximum Tension	Maximum Compression	Data Collection (in thousands of cycles)
2.1	12	7.8 kip 3000 με	-7.8 kip -3000 με	35, 45, 50, 55, 60, 65, 70, 75, 100
2.2	16	9.1 kip 3500 με	-9.1 kip -3500 με	30, 35, 40

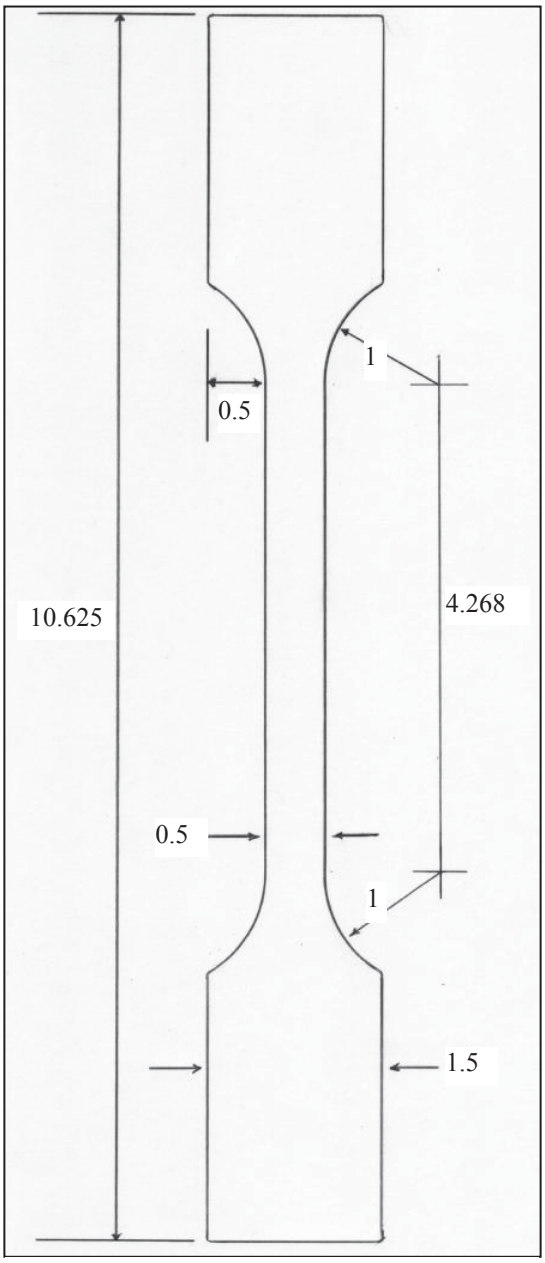

Figure 2.2 Axial specimen design from 0.5 inch thick aluminum flat bar. All dimensions shown are given in inches.

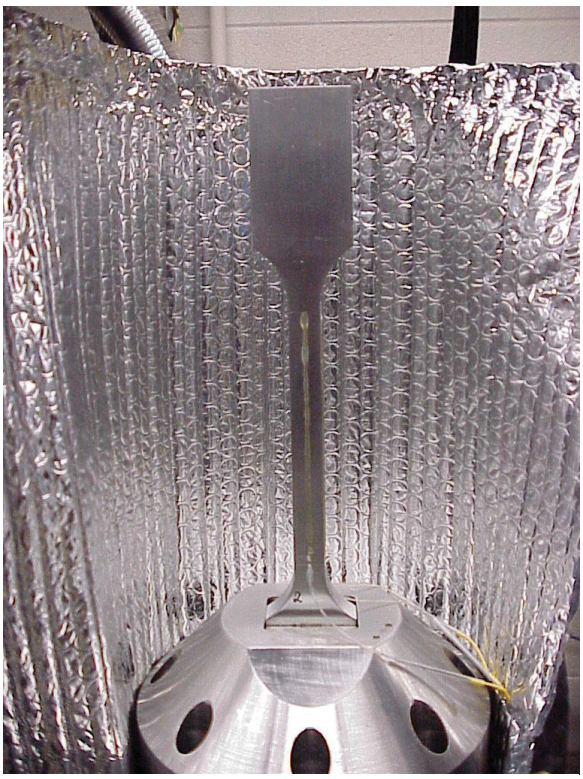

Figure 2.3 Axial specimen mounted in the testing machine, showing the fiber placement and insulating shroud.

Both specimens were equipped with two strain sensing optical fibers attached to opposite sides of the specimen. With Specimen 2.1, each fiber had six FBG sensors in the glue line. Thus, a total of 12 sensors were monitored with that one specimen alone. With Specimen 2.2, each fiber had eight sensors in the glue line, giving a total of 16 sensors. Additionally, a third fiber was attached to the side of each specimen using a small diameter tube to mechanically decouple it from the specimen. This fiber was intended to measure temperature; however, this approach did not adequately decouple the fiber from the strain that the specimen experienced and could not be used reliably for its intended purpose. However, an aluminum insulating shroud was used to protect the specimens from transient environmental effects while measurements were taken (see Figure 2.3).

The fatigue tests were conducted as follows. The specimens were mounted in the hydraulic grips of the MTS testing machine, and data was collected during holds at zero load, at the given tensile load, and then at the given compressive load. Considering the slow sample rate, these holds were sustained for several minutes each in order to acquire a statistically significant amount of data (at least 100 separate scans per hold). Then the specimen was subjected to mechanical fatigue cycles as described above. Periodically, the test was halted for data collection, and during these times the specimen was again held at these same three loads (0 kip, tension, compression). This data collection was conducted according to the schedule in Table 2.1.

2.3 Results

The initial strain data collected during the first no-load, clamped hold (prior to any mechanical cycling) is not considered representative of the conditions present for the duration of the test, because it is apparent (and not uncommon in this type of dynamic mechanical testing) that the loading conditions changed slightly during the first few thousand cycles of testing. These changes are due to a combination of factors which over the course of a few thousand cycles settled into a stable condition. These factors include such things as alignment and positions of the two gripping wedges in both of the two hydraulic grips. These things are difficult if not impossible to control precisely when testing a specimen of this size. Thus, one must report the actual conditions of the test, and use these in the analysis of test results. Therefore, the results of this fatigue test will be referenced to conditions after the first scheduled stoppage at around 30,000 to 35,000 cycles (depending on the specimen) rather than actual initial conditions.

Figure 2.4 shows the average strain gradients measured by both strain sensing fibers attached to Specimen 2.1 after completion of 35,000 fatigue cycles. These data are actually the averages of the strain measured by the six FBG strain sensors on each fiber during a hold of over six minutes duration at zero load. While this data set was collected, the specimen was gripped with both hydraulic grips clamped, but the axial load was held constant at zero. Therefore, this figure shows that even under no axial load, the specimen was experiencing a non-zero strain, and a non-zero, linear strain gradient which is consistent with a misalignment in the hydraulic grips of the MTS testing machine. For reference, the full data set for this configuration is shown in Figure 2.5.

Figures 2.6 and 2.7 show the data collected from Specimen 2.1 after 35,000, 60,000, 75,000, and 100,000 fatigue cycles while the specimen was held in tension and compression, respectively. These data sets are chosen because they are representative of those collected at other times during this test.

In figures throughout this chapter, "FBG 1" represents the first monitored strain sensor in the glue line for a fiber, and positioned nearest the lower hydraulic grip. FBG 1 on Fiber 1 was located at approximately the same cross-section as FBG 1 on Fiber 2, but on the opposite side of the specimen. However, this positioning was not controlled precisely. Each consecutive FBG sensor was separated from adjacent sensors by 1 cm (center to center).

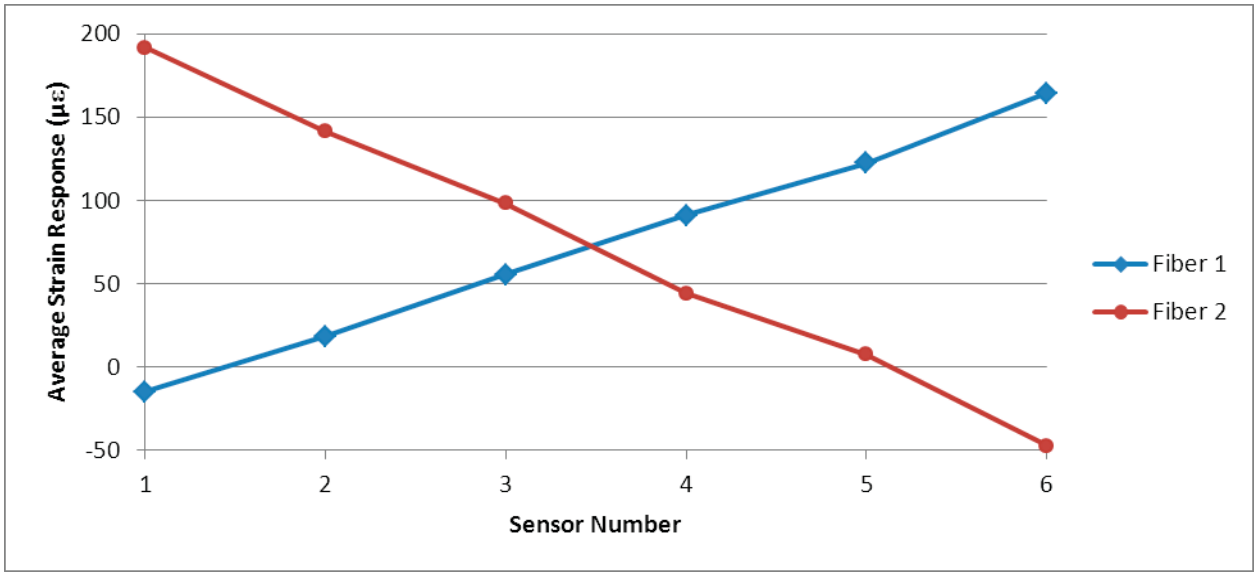

Figure 2.4 The average strain response of the two fibers attached to Specimen 2.1 showing the strain gradients present after 35,000 mechanical cycles. The specimen was held at zero load while these data were collected.

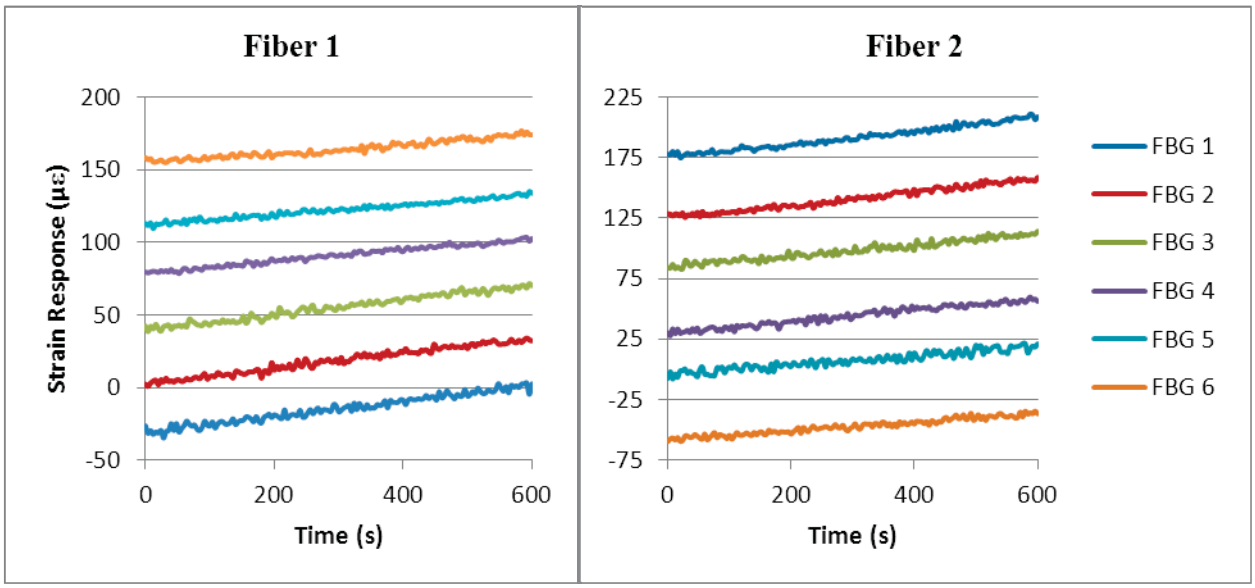

Figure 2.5 The strain response of the two fibers on Specimen 2.1 after 35,000 mechanical cycles during a hold at zero load with both grips clamped. Since the fibers are on opposite sides of the same specimen, the strain gradients (as shown in Figure 2.4) are reversed. FBG 1 on Fiber 1 is located at approximately the same cross-section as FBG 1 on Fiber 2, but on the opposite side of the specimen. However, this positioning was not precisely controlled.

Specimen 2.1 broke shortly after mechanical cycling resumed after collecting data at the 100,000 cycle mark. Just prior to the specimen breaking, a visual inspection of the optical fibers and glue lines was performed, and this did not reveal any visible damage or any evidence of the fiber debonding from the specimen. All of the FBG strain sensors that were monitored on Specimen 2.1 during this test were still functioning and returning the expected strain magnitudes at this point.

Whereas Specimen 2.1 was cycled between +/- 3000 με and failed after just over 100,000 cycles, Specimen 2.2 was cycled between +/- 3500 με and failed at just over 40,000 cycles. Figures 2.8 and 2.9 show the average strain response for the eight FBG strain sensors monitored on each of the two fibers attached to Specimen 2.2 after 30,000, 35,000, and 40,000 cycles. These figures show the average of data sets like those shown in Figures 2.6 and 2.7. Therefore, together these figures show the average strain gradients present on opposite sides of the specimen during holds in tension and compression at three different times during the fatigue test. As in Specimen 2.1, these sensors are separated by a center to center distance of 1 cm.

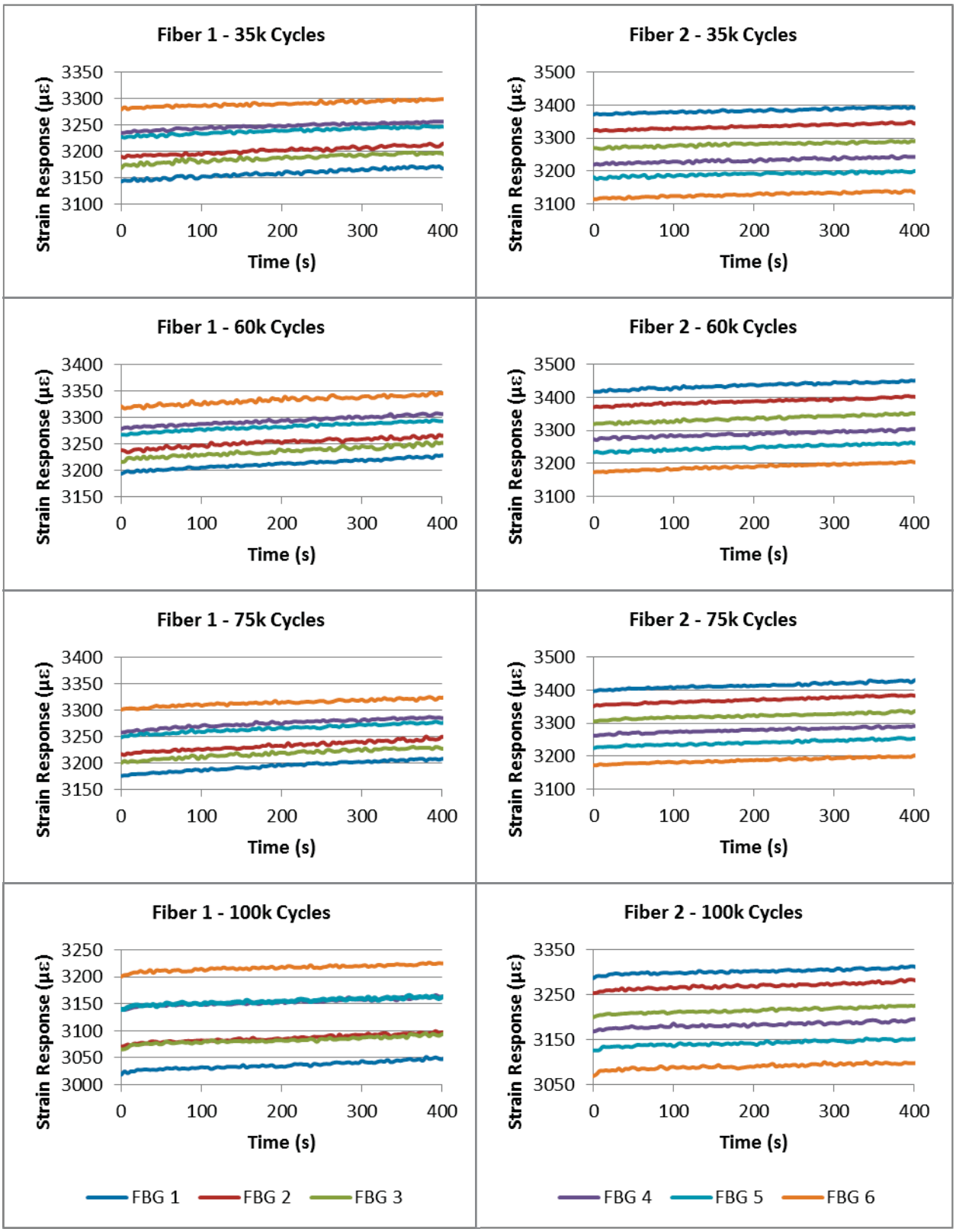

Figure 2.6 The strain response from the six FBG strain sensors on Fiber 1 (left column) and Fiber 2 (right column) of Specimen 2.1. These data were taken at different periods during the fatigue test during tensile holds at 7.8 kip. This behavior is typical of the data collected under similar conditions at other times during the test.

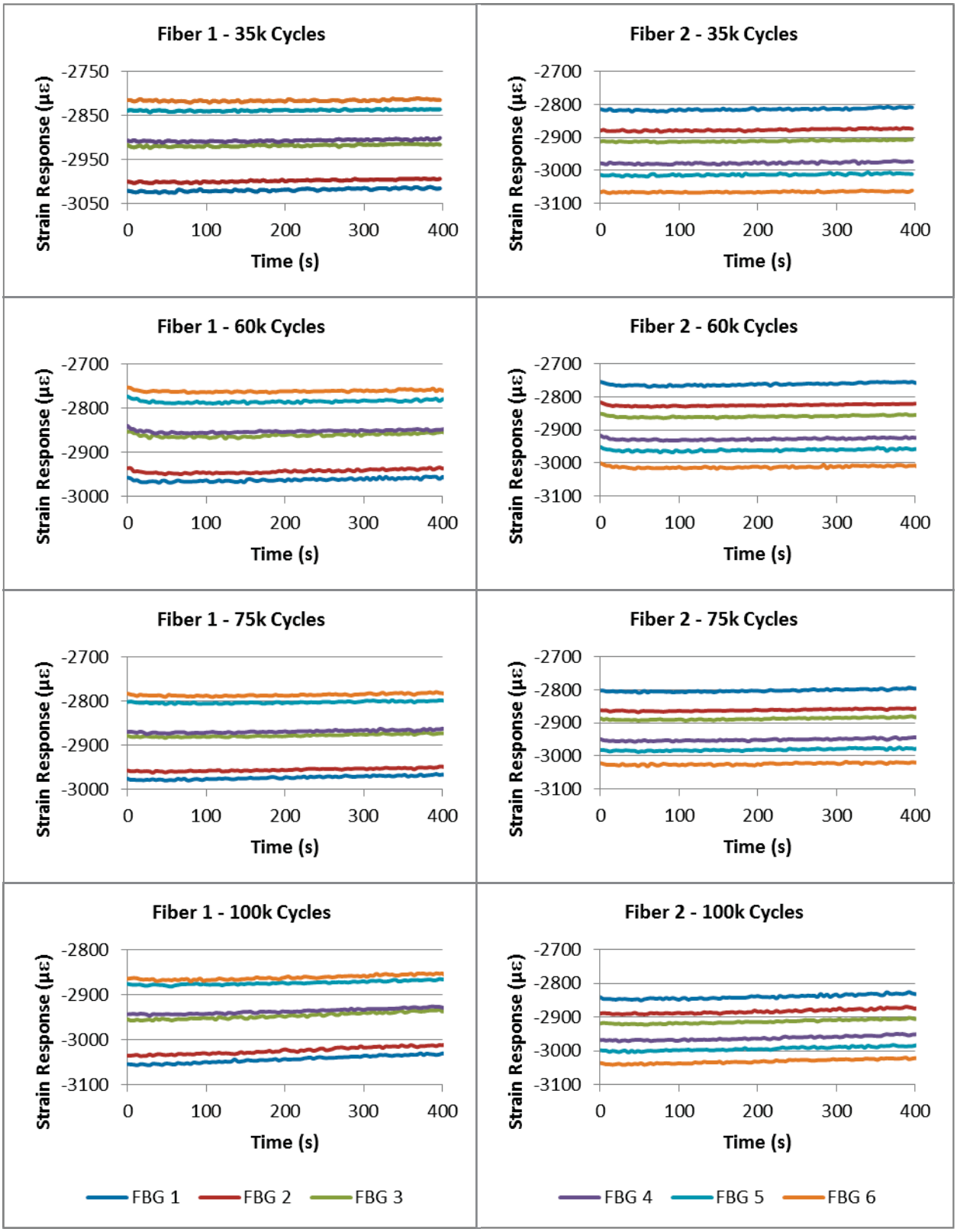

Figure 2.7 The strain response from the six FBG strain sensors on Fiber 1 (left column) and Fiber 2 (right column) of Specimen 2.1. These data were taken at different periods during the fatigue test during compressive holds at -7.8 kip. This behavior is typical of the data collected under similar conditions at other times during the test.

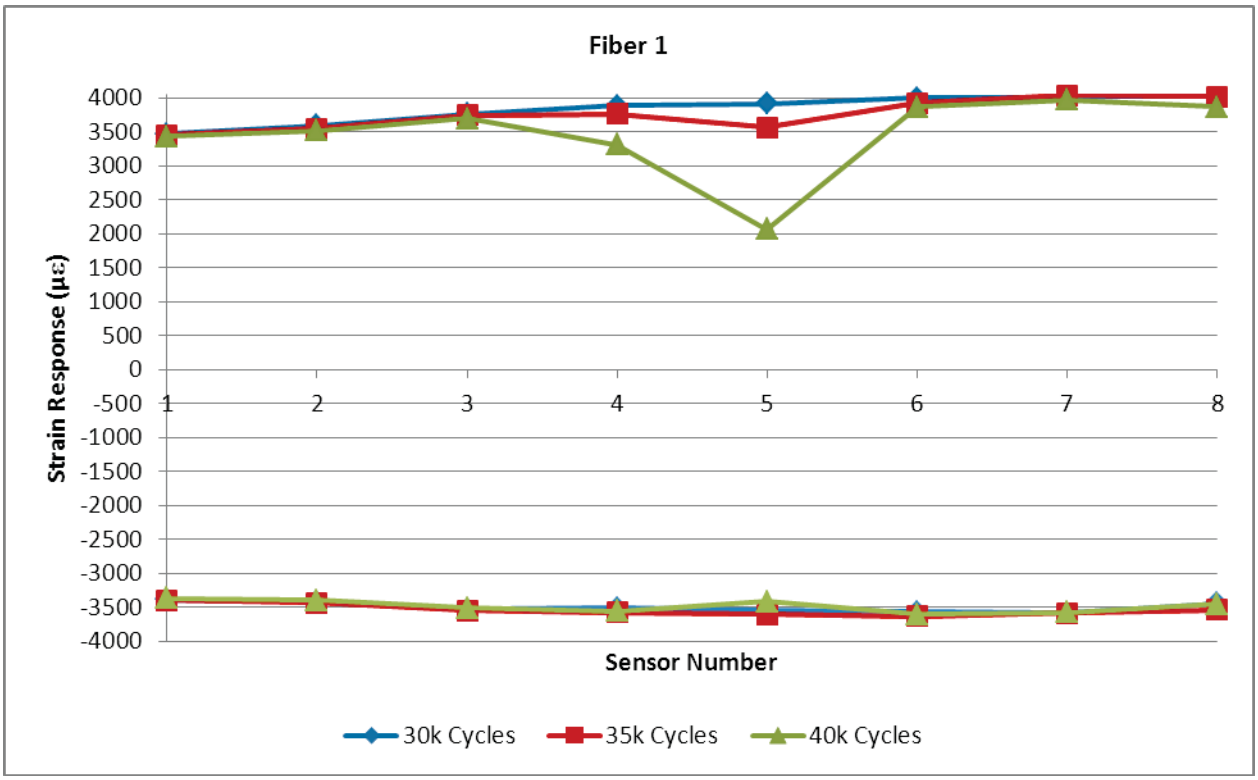

Figure 2.8 The average strain response of the eight FBG strain sensors monitored on Fiber 1 of Specimen 2.2. This shows the strain response in the fiber after 30,000, 35,000, and 40,000 cycles during holds in both tension and compression. The specimen failed shortly thereafter. When in tension, Sensor 5 recorded a drop in strain of over 1800 με at 40,000 cycles.

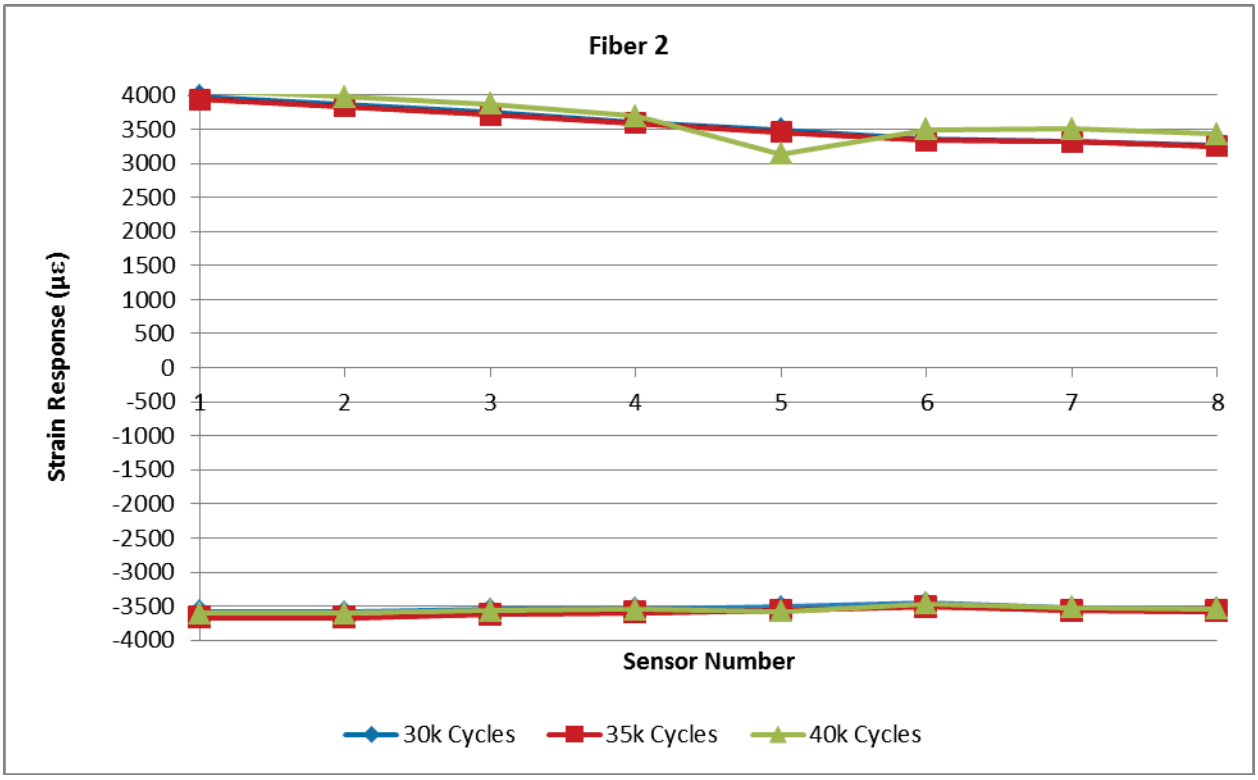

Figure 2.9 The average strain response of the eight FBG strain sensors monitored on Fiber 2 of Specimen 2.2. This shows the strain response in the fiber after 30,000, 35,000, and 40,000 cycles during holds in both tension and compression. The specimen failed shortly thereafter. When in tension, Sensor 5 recorded a drop in strain of almost 400 με at 40,000 cycles.

2.4 Discussion

This axial fatigue test was designed to expose fiber optic strain sensors to a large strain amplitude at a low cycle rate using a hydraulic test machine. In this test, two aluminum specimens – each with two optical fibers containing discrete FBG strain sensors – were mechanically cycled at room temperature in order to determine if fatigue damage would introduce error in the strain response of the sensors. Specimen 2.1 was exposed to sinusoidal fatigue cycles between approximately +3000 με and -3000 με at a frequency of 10 Hz, and Specimen 2.2 was cycled between +3500 με and -3500 με at the same frequency. Thus, these were completely-reversed cyclic fatigue tests, so that each sensor experienced both tension and compression during each mechanical cycle. The tests were halted and the sensors were interrogated periodically according to the schedule given in Table 2.1. Figures 2.6 and 2.7 (from Specimen 2.1) are representative of these data, and show the typical strain response from the 12 strain sensors monitored on this specimen. This was done with the specimen held at maximum tension, maximum compression and also at no load. Data was collected for several minutes each time the test was halted in order to acquire sufficient data for statistical analysis.

Perhaps the first thing to note with these results is that they suggest a slight misalignment in the hydraulic grips of the MTS testing machine. This is evident in the strain gradient observed in almost every data set collected from both specimens (see Figure 2.4, in particular). As this figure indicates, the initial strain gradients measured (with the sensors on Specimen 2.1) were 36 με/cm and -47 με/cm for Fibers 1 and 2, respectively. The difference in sign is expected because the fibers are on opposite sides of the specimen, but the difference in magnitude is unexplained. Possible explanations include a slight misalignment of the fibers with respect to the loading axis of the specimen, slight differences in strain transfer capability for the two different fibers and glue lines, and an unaccounted for error in baseline measurements (the initial unstrained measurements which are deducted from future strain measurements – analogous to balancing a conventional strain sensor). Naturally, the difference is likely due to some combination of these. Since this data set was not inspected until after the test was completed, it is not possible to determine the true cause with any certainty. For reference, the initial strain gradients detected with the two fibers on Specimen 2.2 are -36 με/cm and 32 με/cm for Fibers 1 and 2, respectively.

In fatigue testing there are several issues to consider. First of all, if one were to utilize a reference sensor (or strain gage) that is permanently bonded to the specimen to determine the "actual" strain present during the fatigue test, then it would be impossible to determine if disagreements are due to fatigue damage in the optical fiber sensors or are due to fatigue damage in the conventional strain gage. This creates a real and tangible problem. A second approach, for comparison, might be to temporarily attach a removable strain sensor such as an extensometer. However, this approach presents the problem of maintaining the baseline (or unstrained) strain condition from one measurement to the next. In other words, as soon as one removes the extensometer, it would be practically impossible to reattach it in the same strain condition the next time. So permanently attached sensors present a problem, and removable sensors do as well. Therefore, the approach in this test was assume that initial measurements were correct, and then to compare future results to these initial measurements. Additionally, given the loading conditions and the expected effects of grip misalignment, one would expect a monotonic strain distribution along the loading axis of the specimen. Therefore, the character of the strain profile returned by the optical sensors was analyzed to see if it was consistent with expectations.

Another issue to consider in regard to performing fatigue tests is that the sensor response may be evaluated in many different ways. For instance, the absolute magnitude of the sensor response may be compared to that of a secondary sensor, or to that one should expect for the given loading conditions and specimen design, or to the response that the same sensor gave during an earlier interrogation under similar loading. On the other hand, instead of comparing the magnitude of the sensor response, one could investigate the precision of the sensor response. In other words, one could monitor the level of noise in the signal in order to determine if the quality of the signal is reduced due to fatigue. In this test, both the strain magnitudes and standard deviations of the output from the various optical fiber strain sensors were considered.

The average tensile and compressive strain responses of the six optical fiber sensors on Fiber 1 of Specimen 2.1 are shown in Figures 2.10 and 2.11, respectively, while Figures 2.12 and 2.13 show the average tensile and compressive strain responses of the six sensors on Fiber 2.

Since it seemed to have taken several thousand cycles for the specimen to become fully seated into the grips of the MTS test machine, the end conditions changed during the first few thousand

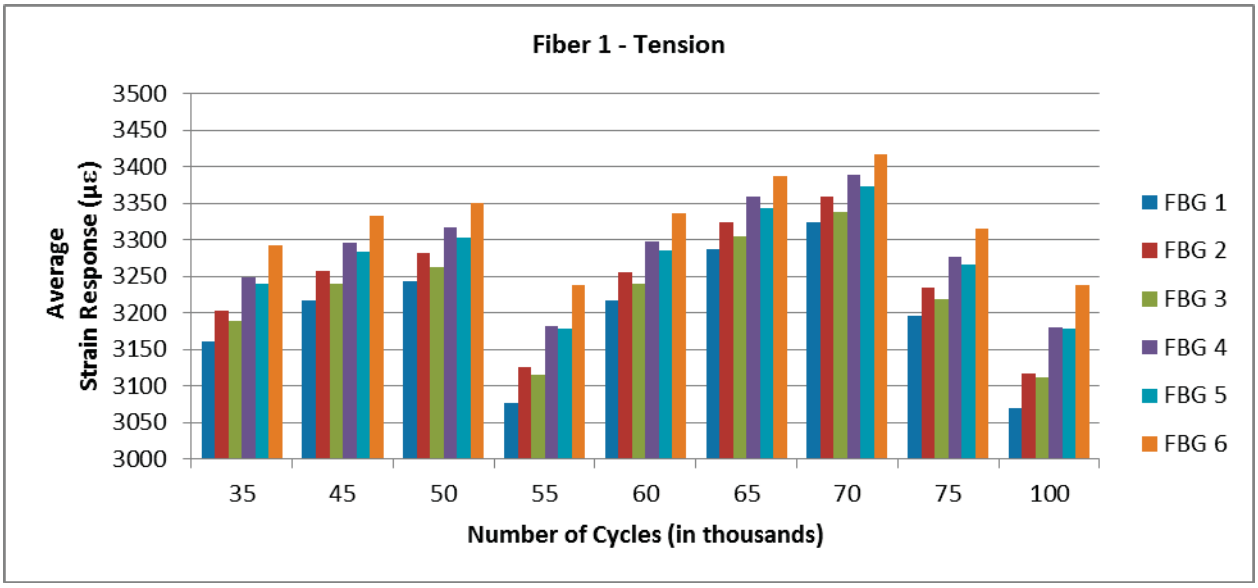

Figure 2.10 The average strain response of the six FBG strain sensors monitored on Fiber 1 of Specimen 2.1 in tension. This figure shows the axial strain profile of the specimen for each of the nine times that the fatigue test was halted for data collection. A strain gradient is obvious and persistent. However, the strain profile was not monotonic for this fiber.

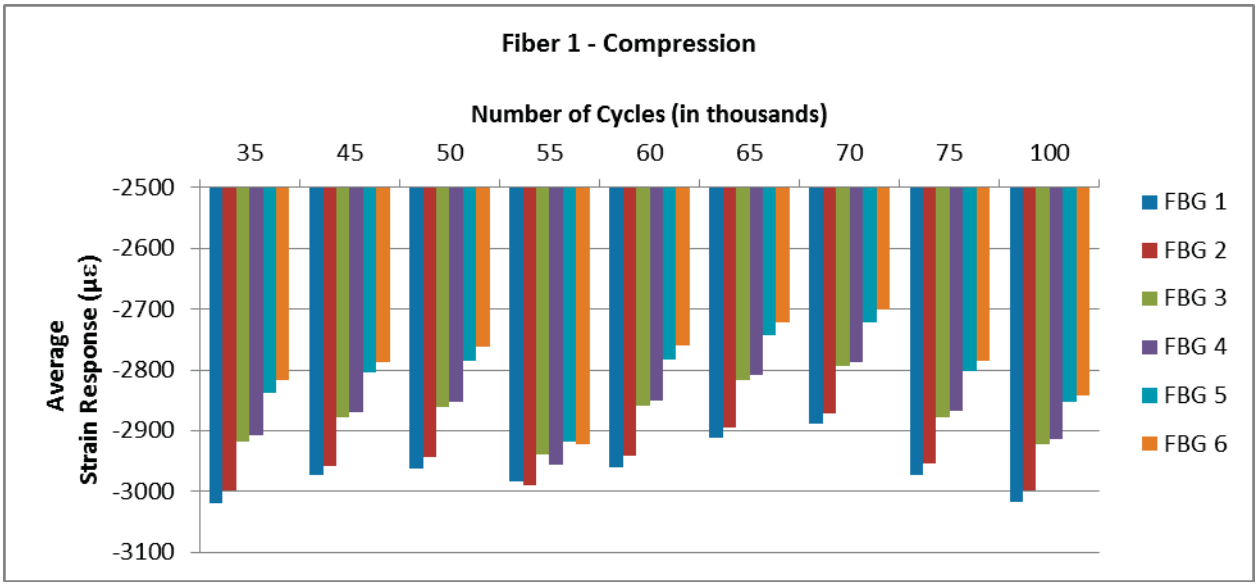

Figure 2.11 The average strain response of the six FBG strain sensors monitored on Fiber 1 of Specimen 2.1 in compression. The strain gradient was evident in compression, as well. However, the profile was irregular in this case.

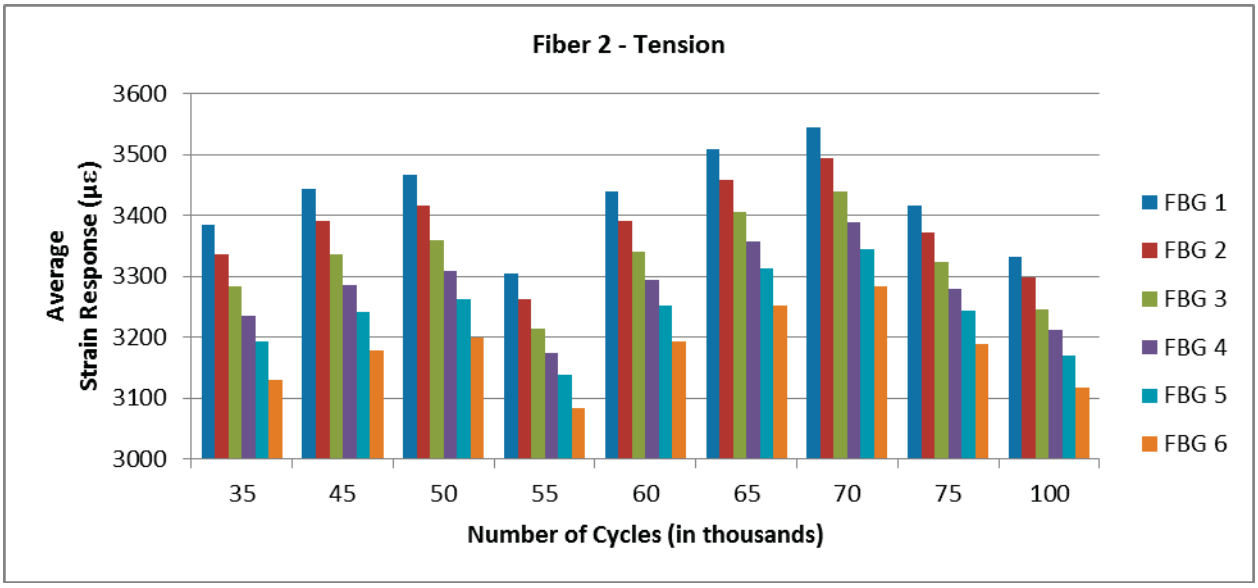

Figure 2.12 The average strain response of the six FBG strain sensors monitored on Fiber 2 of Specimen 2.1 in tension. Fiber 2 for this specimen behaved much better then Fiber 1, showing nice linear, monotonic strain gradients throughout the fatigue test.

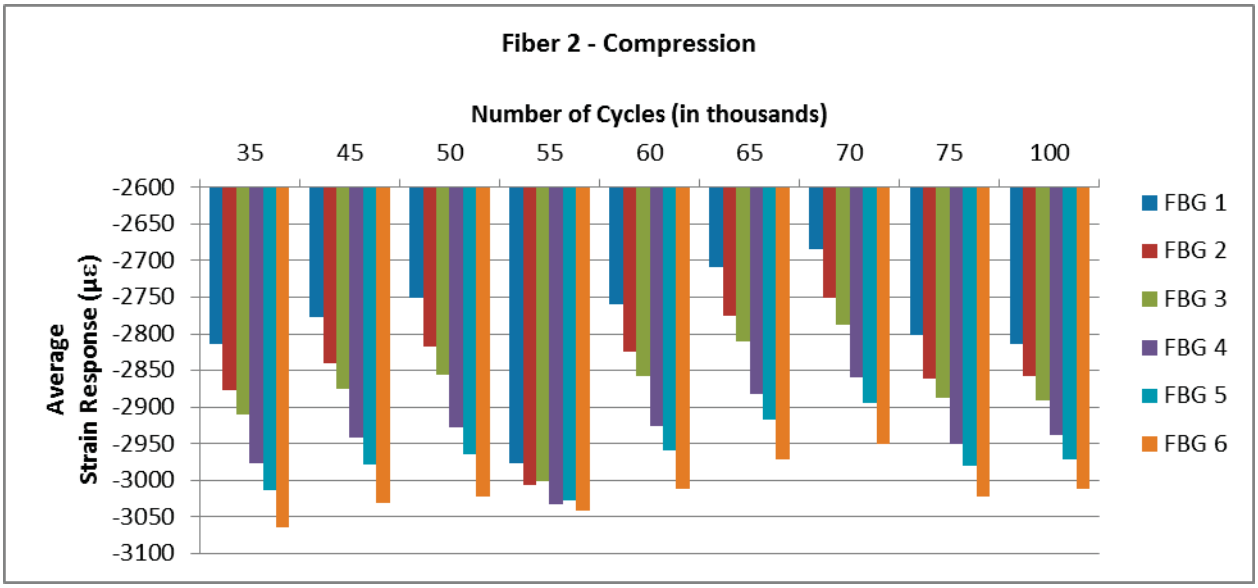

Figure 2.13 The average strain response of the six FBG strain sensors monitored on Fiber 2 of Specimen 2.1 in compression. Aside from the data at 55,000 cycles, this fiber behaved as well in compression as it did in tension.

cycles. This is apparent in the data because it caused the strain profile to change noticeably. Therefore, as mentioned earlier, the strain output for the sensors on Specimen 2.1 will be compared to that of these sensors at 35,000 cycles.

Therefore, the strain data represented in Figures 2.10 through 2.13 become clearer by removing the strain profiles at 35,000 cycles. This is in effect a rebalancing of these sensors by subtracting out a new strain baseline (that acquired at 35,000 cycles). Doing so will make comparing the strain response of these fibers easier, and the results are shown in Figures 2.14 through 2.17. These figures show how the strain response of these sensors varied over the duration of the fatigue test with respect to the strain profile present at 35,000 cycles.

Figures 2.14 through 2.17 indicate that (on Specimen 2.1) both the average strain and the magnitude of the strain gradient varied as determined by the optical fiber sensors. There are several issues which should be considered when evaluating this result. First, the temperature of the specimen (at the time the data was collected) was not controlled. Thus, a change in temperature of the specimen of 11.5 ^{o}F would be sufficient to produce a thermal strain of 150 με (the largest variation observed in this data). This effect cannot be distinguished from non-thermal strain, but should be nominally consistent throughout the specimen because the specimen was enclosed in an insulating shroud. Secondly, the MTS test machine was equipped with hydraulic grips which were warm to the touch due to the warm hydraulic fluid they contained. The grip temperature, and consequently the specimen temperature, would have varied widely during this test. Therefore, the variation observed in these figures is not surprising. Additional testing should be completed with additional sensors to distinguish and account for thermal strain.

The variation observed in the magnitude of the strain gradient is thought to be due to variations in the end conditions imposed by the hydraulic grips. Without removing the specimen from the testing machine (which would introduce other issues), this effect on the strain profile is difficult to distinguish and account for.

Therefore, with these considerations, the sensors on Specimen 2.1 appear to have returned reasonable strain values throughout the duration of this fatigue test. In particular, the strain profiles indicated by these sensors after 100,000 cycles nearly matched that indicated by these same sensors before significant fatigue damage had occurred. In fact, as shown in Figures 2.14 through 2.17, the strain profiles at 100,000 cycles (just before specimen failure) matched that at

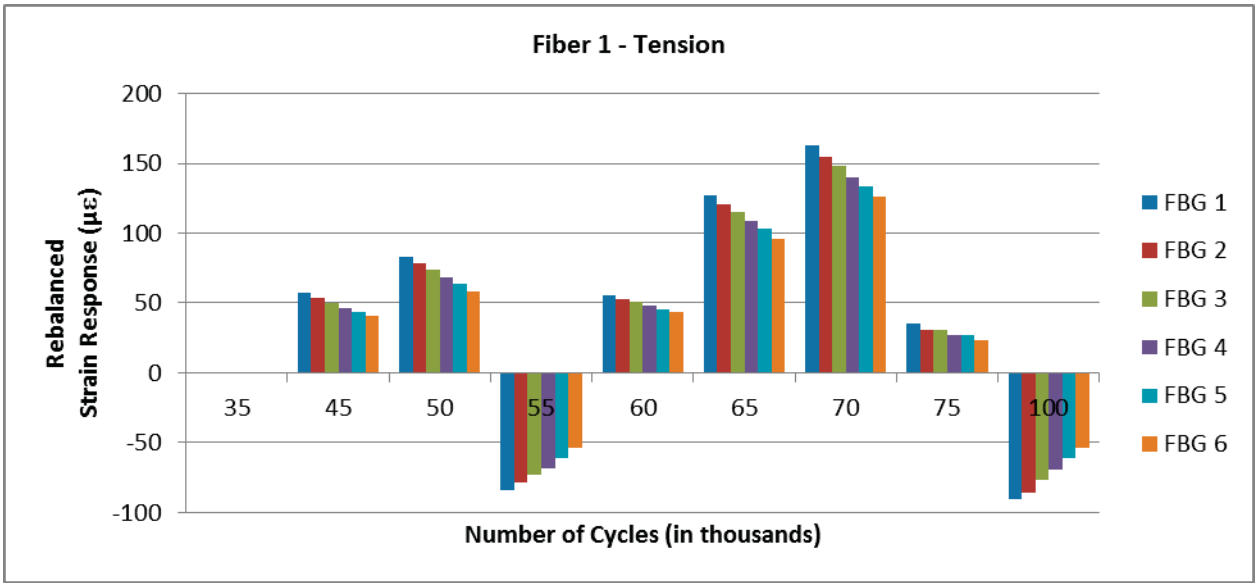

Figure 2.14 The rebalanced strain response of the six FBG strain sensors monitored on Fiber 1 of Specimen 2.1 in tension. This is the data from Figure 2.10 rebalanced by deducting the tensile strain profile determined at 35,000 cycles. This shows how the strain response varied over the duration of the fatigue test.

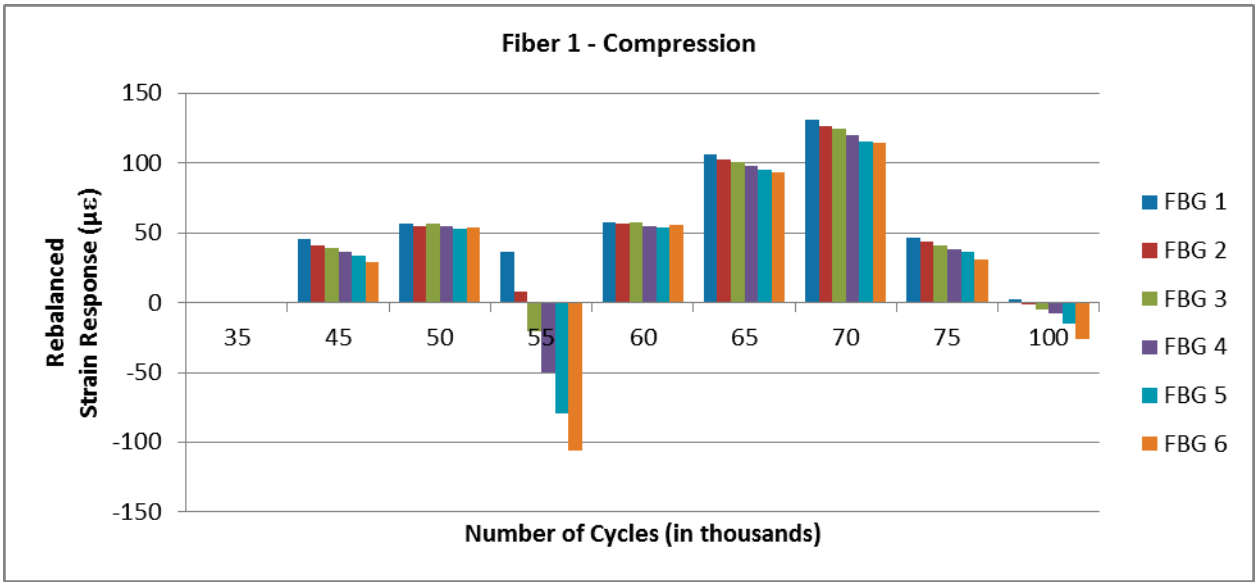

Figure 2.15 The rebalanced strain response of the six FBG strain sensors monitored on Fiber 1 of Specimen 2.1 in compression. This is the data from Figure 2.11 rebalanced by deducting the compressive strain profile determined at 35,000 cycles.

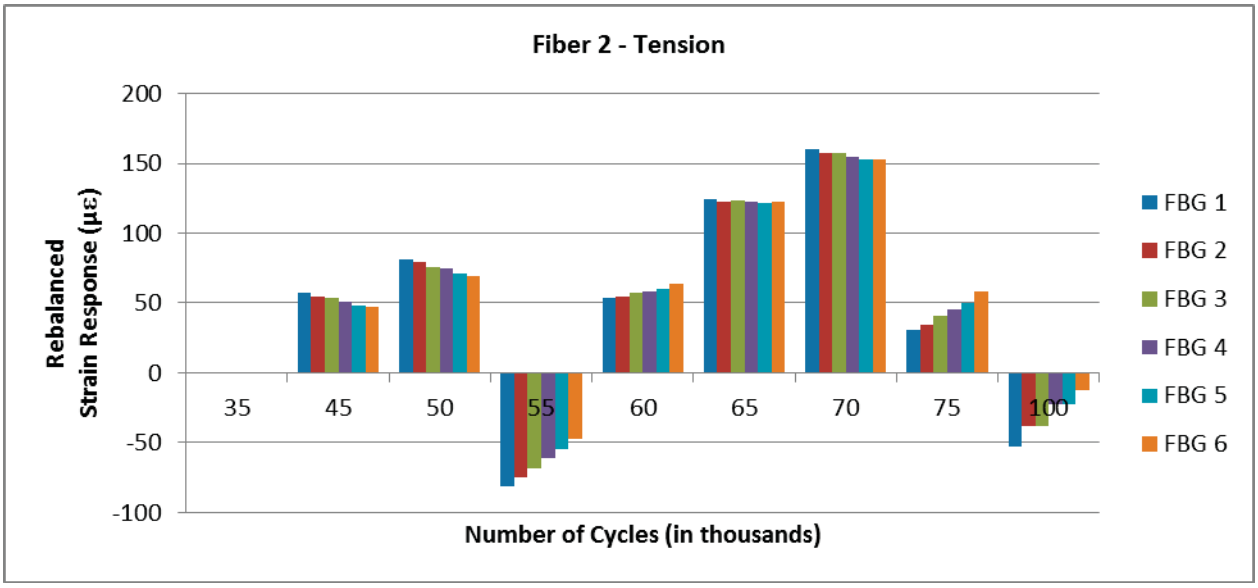

Figure 2.16 The rebalanced strain response of the six FBG strain sensors monitored on Fiber 2 of Specimen 2.1 in tension. This is the data from Figure 2.12 rebalanced by deducting the tensile strain profile determined at 35,000 cycles.

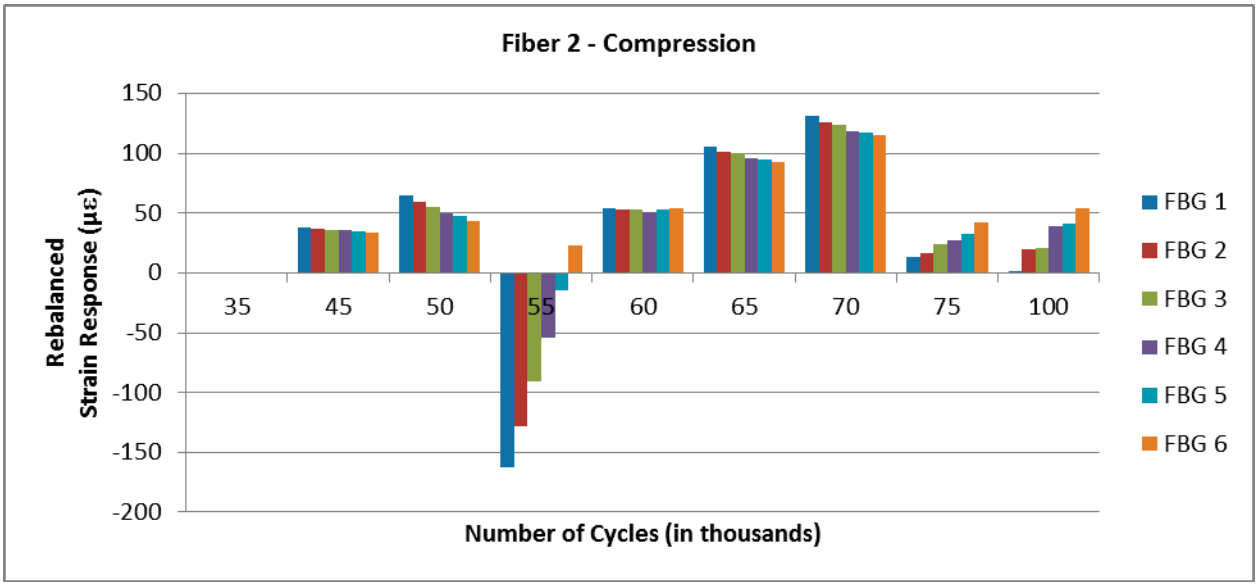

Figure 2.17 The rebalanced strain response of the six FBG strain sensors monitored on Fiber 2 of Specimen 2.1 in compression. This is the data from Figure 2.13 rebalanced by deducting the compressive strain profile determined at 35,000 cycles.

35,000 cycles better than strain profiles observed at several other times in the test (in particular, at 70,000 cycles). Therefore, this data does not indicate a progression and accumulation of fatigue damage.

Furthermore, this fatigue did not produce any detectable damage to the glue line, or to the fiber itself. Clearly, more testing should be done to address the variations observed, but considering Specimen 2.1, this test does not suggest any particular cause for concern.

Unfortunately, this is not exactly the case considering the data from Specimen 2.2. While most sensors on this specimen behaved quite well, three of them returned quite unexpected results – in particular, Sensors 4 and 5 on Fiber 1 and Sensor 5 on Fiber 2. As is evident in Figures 2.8 and 2.9, these sensors indicated an unexpectedly low strain, especially at the 40,000 cycle mark. The largest difference was Sensor 5 on Fiber 1 which indicated strain almost 2,000 με below what was expected, based on nearby sensors and based on the earlier strain profile at 30,000 cycles. The exact cause of this is unknown, but could be the result of fatigue damage in the glue line. However, no observable damage or delamination was detected in the glue line in this region or elsewhere. Furthermore, the specimen did not fail near this cross-section, but rather failed in a cross-section near the end of the glue line of these fibers (closer to Sensor 1). Although it may not be coincidental that these sensors were generally in the same location (i.e. cross-section), to attribute this significant difference to anything other than glue line damage would be speculation. The differences observed in the data from Specimen 2.1 are much smaller in magnitude and are quite consistent with temperature and end condition effects. Unfortunately, that is not the case with the errors observed in the response from these sensors.

The different results from these two specimens suggest that a logical algorithm is needed to determine whether or not the results from each specimen indicate the presence of fatigue-induced errors in the strain response of the various FBG sensors. The algorithm employed in this case was a three point argument, and went as follows:

First, is there a reasonable alternative explanation for the observed strain response? This is based on reasonable variability in certain conditions – such as the specimen temperature, and the end conditions imposed on the specimen by the hydraulic grips – which would be expected to modify the actual strain in the specimen. Such natural variation should not be attributed to error in the sensing system, but may be difficult to distinguish.

Second, does it appear that individual sensors failed separately, or does it appear that all sensors in a given glue line responded in a way that is consistent with the response of the other sensors in that glue line? This is based on the reasonable expectation that an entire glue line would not degrade in the same way throughout its entire length. Thus, one should fatigue damage to affect a few individual sensors, and to affect them by different amounts. One should expect all of the sensors in a given glue line to behave in a similar way only if no fatigue-induced degradation has taken place.

Finally, does the data indicate any sort of trend (for any given sensor) with increasing fatigue? In other words, fatigue damage should accumulate with increasing fatigue cycles. Therefore, the strain response for affected sensors should exhibit a trend from what is expected (based on adjacent sensors, and on known loading conditions) to some clearly erroneous value with increasing fatigue cycles.

The strain response of the sensors on both Specimen 2.1 and 2.2 were evaluated according to this algorithm. In regard to Specimen 2.1, the results are that no fatigue-induced degradation is detectable. For instance, there exists a reasonable alternative explanation for the observed strain – namely, variations in temperature and end conditions. Second, as can be seen in Figures 2.14 through 2.17, all of the sensors in each glue line behaved in a way that was consistent with all of the other sensors in their respective glue line, with no individual sensors responding erratically. Finally, these figures also show that there is no obvious trend with increasing fatigue cycles.

However in regard to Specimen 2.2, the results are less favorable. For instance, there exists no reasonable alternative explanation for the strain response of Sensors 4 and 5 on Fiber 1 (Figure 2.8), nor for that of Sensor 5 on Fiber 2 (Figure 2.9). Furthermore, these three individual sensors have a significantly different strain response than the remaining sensors in those glue lines, which is consistent with what one would expect from fatigue damage. Finally, these figures clearly show that the response of these three sensors appear to degrade with increasing fatigue cycles. Therefore, it was concluded (based on this algorithm) that no fatigue damage was detectable in the response of the sensors on Specimen 2.1. However, this algorithm indicates that out of the 16 sensors monitored on Specimen 2.2 there were three FBG sensors which were returning erroneous results by the time the specimen failed.

In addition to the strain magnitudes returned by these strain sensors, the noise inherent in the signal returned by these sensors was also investigated. Recall in this discussion that this data was acquired at a very low 0.25 Hz. However, with this Distributed Sensing System, the quality of the acquired signal is typically quite good with very little noise.

Using data from Specimen 2.1, it was found that the standard deviation of the strain response signals did not increase noticeably over the 100,000 cycles of this fatigue test. This data is shown in Table 2.2. In fact, it is evident from the data at 100,000 cycles that the signal quality is quite good, with a standard deviation of only around 1.5 με. This is nearly an order of magnitude lower than that of a conventional strain gage which is typically around 10 - 15 με. Since the aluminum specimen failed shortly after this, it is reasonable to expect that the fiber optic sensors were working reliably throughout the life of the aluminum specimen itself.

Table 2.2 Standard Deviations (in με) of Sensors on Specimen 2.1

	FBG 1	FBG 2	FBG 3	FBG 4	FBG 5	FBG 6
Fiber 1 Tension @35k	1.11	1.46	1.90	1.07	1.35	1.76
Fiber 1 Tension @100k	1.46	1.28	0.96	1.45	1.69	1.50
Fiber 2 Tension @ 35k	1.73	1.91	2.41	2.05	1.51	1.71
Fiber 2 Tension @ 100k	1.52	1.85	1.52	1.86	1.36	1.92
Fiber 1 Compression @35k	1.64	0.99	1.25	1.40	1.25	0.85
Fiber 1 Compression @100k	1.17	1.41	2.10	1.25	0.84	1.31
Fiber 2 Compression @ 35k	2.09	1.52	1.41	1.65	2.04	0.98
Fiber 2 Compression @ 100k	1.84	1.58	1.36	1.24	1.84	1.32

The data from Specimen 2.2 are more difficult to analyze in this way because, with these data, several of the sensors were uncharacteristically noisy even before any fatigue cycles were performed. With that specimen, standard deviations as high as 10.43 με were observed in the data from the pristine specimen. However, these numbers actually dropped so that just before the specimen failed at just over 40,000 cycles, the standard deviations ranged as high as only 6.92 με. As confusing as the data from this specimen is, it certainly does not suggest that mechanical fatigue of optical fibers and adhesives will reduce the quality of the strain response of these optical fibers.

Although this discussion pertains to a fatigue test performed on only two specimens, each with two fibers in two separate glue lines, the results are typical of that observed from many other

fatigue tests by the author which were conducted over the course of several years. In this particular fatigue test, a total of four fibers, with a total of 28 FBG strain sensors were evaluated in mechanical fatigue (under tension, compression and no load). So even though the testing involved only two specimens, the number of individual strain sensors evaluated was significant. In each of the fatigue tests conducted to date, the specimen (to which the fiber sensors were bonded) failed before any optical fiber debonded from the specimen, and before any optical fiber failed.

2.5 Conclusions

Naturally, this test did not compare the strain magnitudes returned by these sensors to the actual strain in the specimen (determined by some sort of independent sensors). As discussed, this is an inherent limitation of this type of testing. For how does one objectively determine the "actual strain" in the specimen? With another sensor? If so, then how does one verify that this other sensor has not experienced degradation due to the imposed fatigue? The objective with this test was to compare the strain response from the optical fiber sensors collected at various times during fatigue testing to that obtained from these same sensors prior to any significant amount of fatigue under similar loading conditions. Unfortunately, in this test it was not possible to verify that the loading conditions were precisely the same. However, aside from variations in thermal strain, the loading conditions should not have changed much during the duration of the test.

Since the strain profile determined by the sensors on Specimen 2.1 after 100,000 cycles (and just prior to specimen failure) matched (typically within a few dozen microstrain) that measured near the beginning of the test (i.e. after 35,000 cycles), this test does not suggest cause for concern regarding the durability under fatigue loading of these optical fiber sensors. Specifically, the data from Specimen 2.1 do not indicate any progressive accumulation of fatigue damage.

However, the data from the other specimen used in this test (Specimen 2.2) does suggest that some fatigue damage may have accumulated near three sensors. In fact, just before specimen failure (at around 40,000 cycles) one sensor on this specimen returned a strain magnitude that was almost 2,000 με too low, considering the strain response of nearby sensors and the expected strain profile.

It should be noted again that Specimen 2.1 (which did not conclusively indicate the accumulation of fatigue damage) was cycled between +/- 3000 με, whereas Specimen 2.2 (which did indicate that some fatigue damage might have accumulated) was cycled between +/- 3500 με. It is not clear if this alone is the reason that these sensors malfunctioned, but it may be that this strain level is the limit for the long term durability of this type of optical fiber glue line. Perhaps other adhesives and bonding techniques will provide better life at higher strain amplitudes.

Although, by itself, this test does not fully characterize the durability of optical fiber strain sensing systems, it does provide reason for confidence in the durability of these sensors – at least for fatigue loads below approximately 3,000 με. In fact, in this case, all of the sensors monitored were performing to expectations at the time (or actually just before) the aluminum to which they were bonded failed (at just over 100,000 cycles). For instance, a visual examination of the sensors just prior to the fatigue failure of the aluminum specimen did not reveal any debonding of the fiber sensor, and all of the FBG sensors monitored during this test were operational at that time as well. In this test, each of the six FBG strain sensors monitored from each of the two optical fibers tested outlasted the 7075-T651 aluminum specimen to which they were bonded.

Chapter 3

The Effects of Adhesive Geometry and Type on Strain Transfer for Optical Fiber Strain Sensing

Abstract

The strain response of both acrylate and polyimide coated optical fiber strain sensors bonded to aluminum specimens with M-Bond AE-10, M-Bond AE-15, and M-Bond 200 strain gage adhesives was investigated with both axial and cantilever beam tests. These results were compared to both the strain response of conventional strain gages and to model predictions. The results indicate that only about 82.6% of the known strain in the specimen was transferred through the glue line and fiber coating into the fiber. Thus, multiplying by a strain transfer factor of approximately 1.21 was sufficient to correct the optical fiber strain output. This effect was found to be independent of the adhesive used, independent of the optical fiber coating used, and was also found to be independent of the three-dimensional profile of the glue line used to attach the optical fiber.

3.1 Introduction

Although the durability (during cyclic fatigue) of optical fiber and the adhesive used for mechanical attachment are critically important for strain sensing applications, another important issue which should be considered is the transfer of strain through the adhesive and fiber coating into the fiber core where strain is actually measured. Since neither the fiber coating, nor the strain gage adhesive are rigid materials, they should not be expected to be capable of transferring 100% of the actual strain (at the surface of the specimen) into the optical fiber. Instead, it is expected that both the adhesive and the fiber coating will deform due to the state of shear stress that will naturally result in those layers when the specimen is loaded. So then the pertinent

questions are, how much strain is transferred, and does this depend on the type of adhesive used, on the geometry of the glue line, or on the type of fiber coating? Furthermore, does this depend on whether the specimen is in tension or in compression?

Therefore, the purpose of these tests was to address these questions, and experimentally determine the strain transfer factor(s) necessary to convert optical fiber strain outputs into actual applied strains (as determined by other known and controlled factors). Thus, a series of mechanical tests was performed on various aluminum specimens which were instrumented with optical fiber (both acrylate and polyimide coated) using various common strain gage adhesives.

3.2 Testing Methods

Specimen Design

The first specimen used in this series of tests (see Figure 3.1) was constructed of 38.1 mm wide by 12.7 mm thick (1.5 in wide by 0.5 in thick) 7075-T651 aluminum flat bar. The elastic modulus of this material is reported to be 71.7 GPa (10,400 ksi). The overall specimen length was 270 mm (10.625 in). However, a 114.3 mm (4.5 in) long test section was milled into the central portion. This test section was 12.7 mm by 12.7 mm (0.5 in by 0.5 in) square in cross-section. Thus, the test specimen had the shape of a square dog bone. To this specimen, a length of single mode, acrylate coated optical fiber was bonded using conventional M-Bond AE-10 strain gage adhesive (which was allowed to cure overnight at room temperature). In order to ensure a small uniform glue line, the adhesive was applied to the fiber using a 22 gauge syringe which had been blunted by removing the sharp point. This fiber contained a single continuous fiber Bragg grating (FBG) written into the core of the fiber along its entire length. Since the fiber was attached to the specimen oriented axially along the length of the test section, this configuration permitted one to use the fiber to measure and isolate axial strain in the specimen along the surface to which it was bonded. The length of fiber attached to the specimen's test section was approximately 101.6 mm (4 in) long.

In addition to the optical fiber, a single conventional (resistance) strain gage (CEA-13-125UW-350) was also bonded to the central portion of the test section using the same adhesive and cure cycle. This strain gage was attached to the side of the specimen opposite the optical fiber. Prior to attaching either resistance strain gages or optical fiber, the test section was sanded and

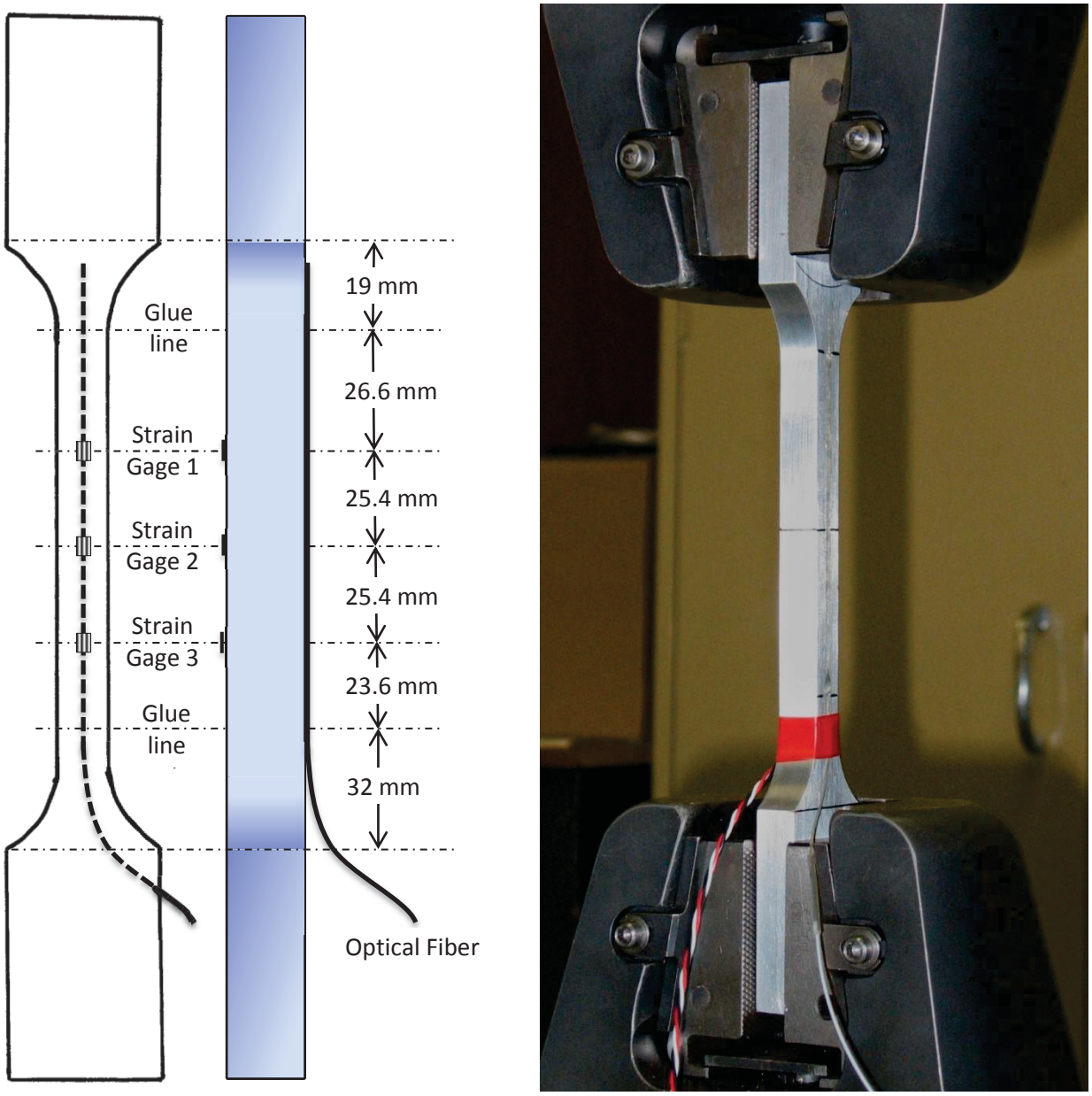

Figure 3.1 Configuration of Specimen 3.1. Note the optical fiber and the three conventional strain gages on opposite surfaces.

thoroughly cleaned according to conventional strain gage adhesive practice. Then sensors were applied according to Vishay Instruction Bulletin B-137 (with the exception that no clamping force was used during the overnight cure cycle). Naturally, some modification to these instructions was necessitated in the application of the optical fiber since these instructions were intended for applying foil strain gages.

After some initial testing, this same specimen was sanded and cleaned again (carefully so as to avoid removing or damaging the existing sensors), and two additional resistance strain gages (also CEA-13-125UW-350) were attached using the same procedure and adhesive technique. This specimen (with its new sensor configuration) is referred to as Specimen 3.1. All resistance strain gages were uniaxial in design and oriented to measure axial strain in the specimen on the surface to which they were attached. The location of each of these sensors is shown in Figure 3.1. All strain gage electrical connections were soldered using 0.56 mm (0.022 in) diameter 62/32/2 resin-core, silver bearing solder.

Another specimen used in this testing, and referred to as Specimen 3.2, was constructed from the same 7075-T651 aluminum flat bar as Specimen 3.1. In fact, aside from sensor configuration, Specimen 3.2 was geometrically identical to Specimen 3.1. However, this specimen was designed to investigate the effects that a smaller, more uniform glue line profile (or cross-section) for the optical fiber and a different strain gage adhesive might have on the strain transfer from the aluminum substrate into the fiber core. Therefore, this specimen was configured with a single continuous-grating, acrylate-coated optical fiber which was bonded with multiple glue lines using two different strain gage adhesives (see Figure 3.2).

As can be seen in the figure, the optical fiber was bonded in one 44.5 mm (1.75 in) long section with AE-10 adhesive, and in another 44.5 mm (1.75 in) long section with M-Bond 200 adhesive. For reference purposes, the extra length of the fiber was wrapped around the specimen to the opposite side, and bonded along a section of approximately 66.8 mm (2.6 in) with M-Bond 200 adhesive. Each glue line was applied with a technique which differs from that used for Specimen 3.1, and as a result, the cross-section for each glue line on Specimen 3.2 was more uniform and much smaller than that of Specimen 3.1. In this case, instead of using a 22 gauge syringe, the adhesive was applied by first placing a small drop of adhesive at one end of the desired glue line

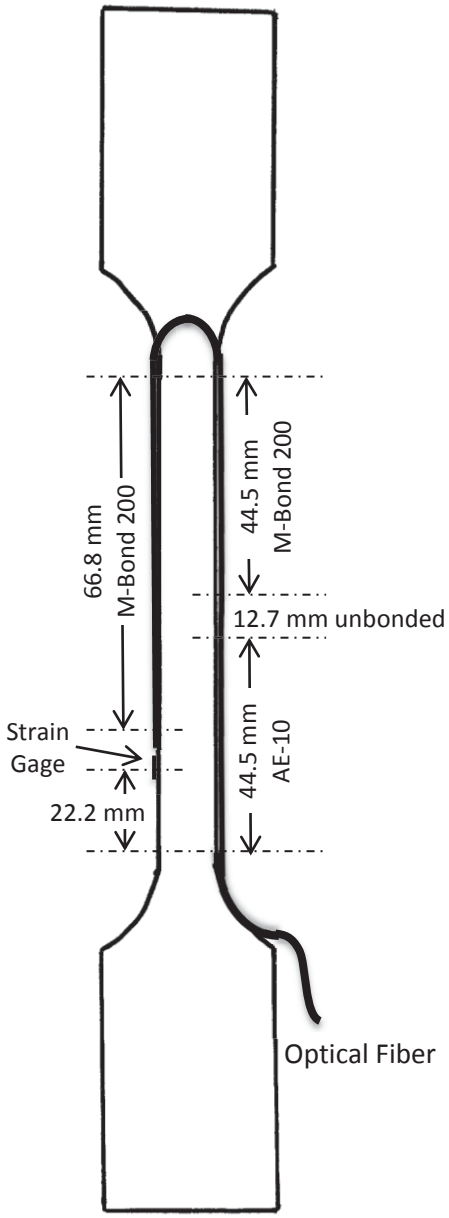

Figure 3.2. Configuration of Specimen 3.2. Note the optical fiber (containing three glue lines) and a single strain gage on the edges of the specimen.

location (right on top of the pre-placed optical fiber). Then the adhesive was wiped down the fiber with a small squeegee made from a short section of general-purpose automotive windshield wiper blade. To avoid mixing of adhesives, a different squeegee was used for each glue line. This process resulted in a small, fine glue line of uniform cross-section which did not extend above the optical fiber.

In addition to the optical fiber, this specimen was configured with a conventional strain gage (CEA-13-125UW-350) which was attached with M-Bond 200 adhesive. The location of this gage is shown in Figure 3.2. As with Specimen 3.1, this specimen was prepared according to conventional strain gage adhesive practices, and the sensors were applied according to Vishay Instruction Bulletin B-137. All strain gage electrical connections were soldered using 0.56 mm (0.022 in) diameter 62/32/2 resin-core, silver bearing solder.

In order to determine the strain transfer factor for a polyimide coated optical fiber, a single optical fiber was bonded to a flat 7075-T651 aluminum specimen (see Figure 3.3). This specimen is referred to as Specimen 3.3. In addition to the optical fiber, a single conventional strain gage (CEA-13-125UW-350) was also bonded to the specimen. The adhesive used throughout was AE-15 mixed and cured (at 175 ^{o}F for one hour) per Vishay instructions. Surface preparations were also completed per Vishay instructions. In the glueline, the optical fiber contained seven conventional 4.6 mm long fiber Bragg gratings (FBG's) which were spaced along the fiber at a center-to-center distance of nominally 10 mm. However, the response from only the center 3 mm of each grating was used in the analysis. Thus, the optical fiber strain data from each grating resulted in 62 data points which were separated by approximately 48 microns (0.048 mm). For each frame of each 24 second scan, this data was averaged to produce a single number from each grating. (Each scan collected data for approximately 24 seconds at a nominal sample rate of 167 Hz, and resulted in 4001 individual frames or snapshots.) The strain gage was selected in order to match the coefficient of thermal expansion of the aluminum specimen (13.1 $\mu\varepsilon/^{o}$F). Finally, the strain gage was positioned on the specimen adjacent to the second FBG sensor, and its 3.175 mm (0.125 in) gage length was approximately equal to the 3 mm length portion of the FBG sensor that was used in this analysis. The strain gage was separated horizontally from the optical fiber by 12.7 mm (0.5 in).

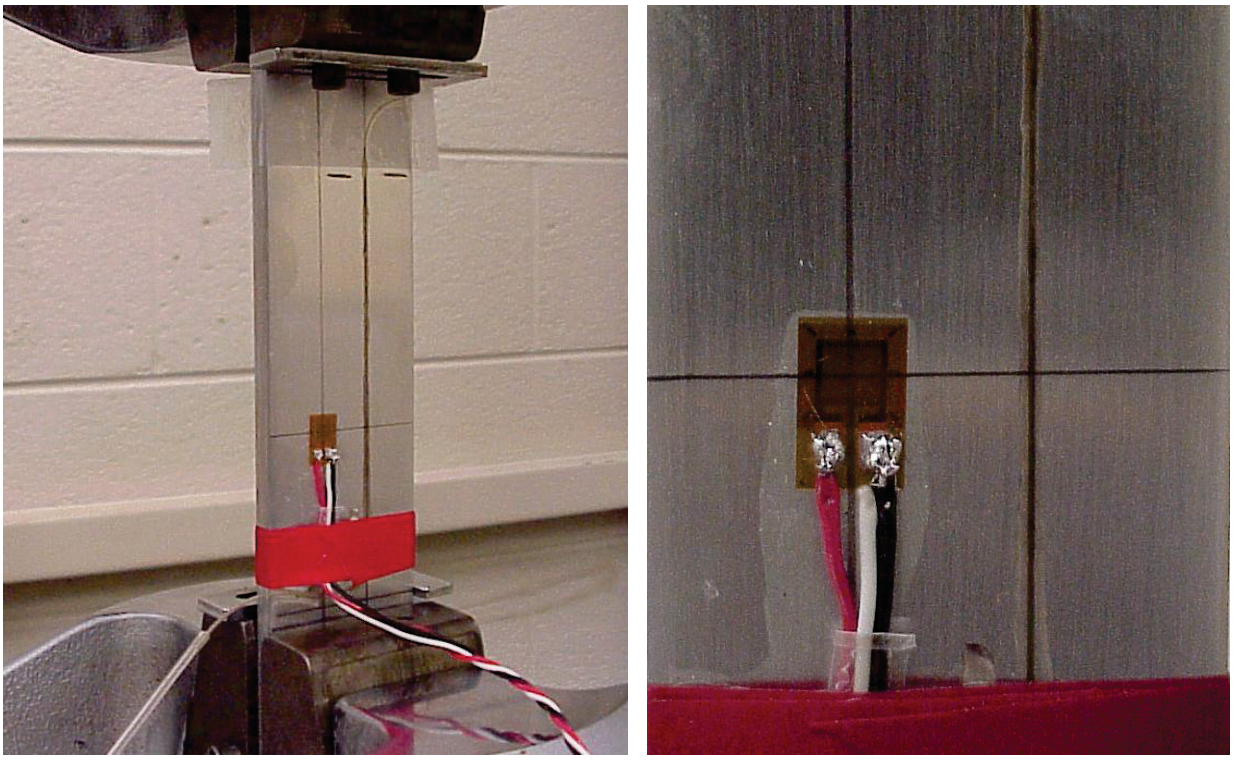

Figure 3.3 Configuration of Specimen 3.3. This specimen was 1.5 in wide by 0.25 in thick with a 4.5 in length between the grips. Note the optical fiber and the single conventional strain gage on the same surface. This optical fiber contained discrete Bragg gratings. Seven gratings were found within the glue line with the second grating adjacent to the conventional strain gage.

In each of these specimens, the ingress of the optical fibers was protected by enclosing the fiber in a length of flexible tubing which was attached to the optical fiber assembly by inserting it under the heat shrink tubing at an adjacent fusion splice. The sensing region of the fiber extended beyond the end of the flexible tubing, and the tubing itself was permanently fixed to the specimen using strain gage adhesive. In this way, the flexible tubing acted as a stress-relief for the optical fiber and effectively protected it from breakage. However, this caused the optical fiber to exit the tubing a short distance away from the specimen surface (due to the thickness of the tubing wall). Therefore, before applying adhesive, the fiber was taped to the specimen surface with a thin strip of tape in order to ensure that the fiber was in contact with the specimen surface.

Testing Machines and Test Equipment

In order to interrogate the strain sensing optical fiber in these specimens, a High Speed Distributed Sensing System (HSDSS) on loan from the Blacksburg, VA facility of Luna Technologies was used. The particular system used in this testing was a DSS 8600B, and contained features and capabilities which were, at the time, still under development. This system was designed to interrogate optical fiber containing a continuous Bragg grating, and was capable of returning individual strain readings from along the sensing fiber with a spatial resolution of approximately 0.0899 mm. This system was capable of scanning and collecting data at several hundred Hertz. However, in these tests, data was collected at 200 Hz. The software used to operate the HSDSS (also on loan from Luna Innovations) was DSS 8600 v0.3 beta.

The resistance strain gages and the load cell output from the testing machines were monitored using a National Instruments CompactRIO 9014 (cRIO) data acquisition system which utilized a NI 9219 signal conditioning and data acquisition module. This system collected data simultaneously from all active channels at 100 Hz. Prior to mechanical testing, load cell and shunt resistor calibrations (using a 100 kΩ shunt resistor) were performed according to normal laboratory procedures.

Specimens 3.1 and 3.2 were tested under axial loading using an MTS 880 Material Test System which consisted of a 22 kip load frame which was computer controlled using an MTS FlexTest SE. Additional tension testing was performed on Specimen 3.3 using another 22 kip MTS load frame controlled by an MTS 407 controller.

Testing Procedures

In order to investigate the transfer of strain from a structural component through the adhesive and the optical fiber coating, an axial tension test was conducted using Specimen 3.1 and an MTS 880 load frame (see Figure 3.1). Prior to mounting the specimen into the machine, baseline strain measurements were collected with both the HSDSS and the cRIO data acquisition systems with the specimen lying flat on a table. The purpose of this was to objectively determine the strain profile for both the optical fiber and the three conventional strain gages with the specimen in an unloaded condition. The simple axial test was conducted in load control mode, and

consisted of a linear ramp (at 3.4696 kN/s) from zero load to 17.348 kN, followed by a short hold and a linear ramp (at the same rate) back to zero load. The hydraulic grips of the MTS were set to 2000 psi.

Additional testing of the strain transfer effect was conducted by performing a cantilever beam test on Specimen 3.1 by loading it transversely. To this end, the specimen was clamped to a table as shown in Figure 3.4 with the optical fiber on the top surface, and known weights were hung as indicated. This was conducted twice – first with a 30.4 lb weight and then with a 43.8 lb weight. This transverse load introduced a linear strain gradient which was then modeled and compared to the strain measurements acquired by both the HSDSS and the cRIO. For each cantilever beam test, the strain was modeled using the following strength of materials relationship:

$$\varepsilon = \frac{6F}{Et^3}x$$

where F is the applied transverse load, E is the elastic modulus of the material, t is the thickness of the beam (parallel to the load), and x is the distance along the axis of the beam from the point of application of the load. Thus, the strain varies linearly, and the strain gradient is simply the coefficient on x in this equation.

Once the strain transfer factor was determined using Specimen 3.1, Specimen 3.2 was assembled with different (smaller, more uniform) optical fiber glue lines and with two different strain gage adhesives as described earlier. The purpose of this test was to determine if different adhesives and/or glue line profiles might alter the strain transfer capabilities and thus require a different strain transfer factor than that found with Specimen 3.1. Therefore, a second cantilever beam test was conducted – this time on Specimen 3.2. In this test, the specimen was mounted and loaded as

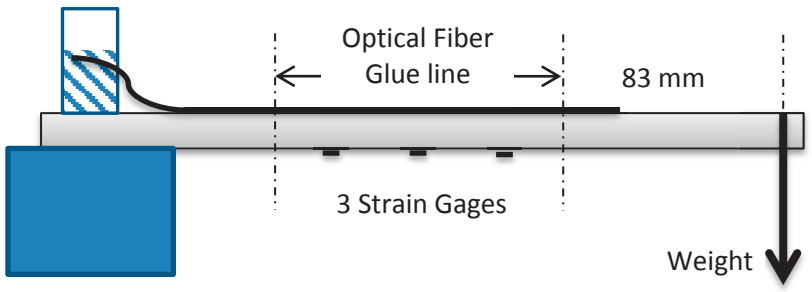

Figure 3.4 Cantilever beam loading of Specimen 3.1.

shown in Figure 3.5 with a series of known weights. The test was conducted with weights of 8.04 lb, 16.28 lb, 30.4 lb, and 43.8 lb. The resulting strain gradients were modeled and compared to the strain measurements acquired by both the HSDSS and the cRIO.

In order to investigate the strain transfer effect with polyimide coated optical fiber, Specimen 3.3 was mounted in a 22 kip MTS load frame controlled by a MTS 407 controller, and loaded from no load to a tensile load of approximately 6500 lb at a constant rate of 325 lb/sec.

3.3 Results

The first and most fundamental element of this portion of the project was to investigate the transfer of strain from a structural component through the glue line and optical fiber coating into the fiber core where strain is actually measured in optical fiber strain sensing applications. The first attempts at this were conducted using Specimen 3.1 under axial loading using the MTS 880 load frame. However, these tests were somewhat inconclusive because the results suggested that the hydraulic grips of the load frame may have been slightly misaligned in such a way that they imposed both a shear and moment load on each end of the specimen in addition to the simple axial load that was intended. Since these additional end conditions were of unknown magnitude, it was determined that this sort of axial test may not be the most suitable for this purpose.

Therefore, in order to investigate the strain transfer issue, a cantilever beam test was conducted using Specimen 3.1 and known weights of 30.4 lb and 43.8 lb. Figure 3.6 shows the strain output from the optical fiber sensors for this test. This strain data was smoothed (in space using an unweighted, five-point moving average), and the smoothed data is what is shown in the figure.

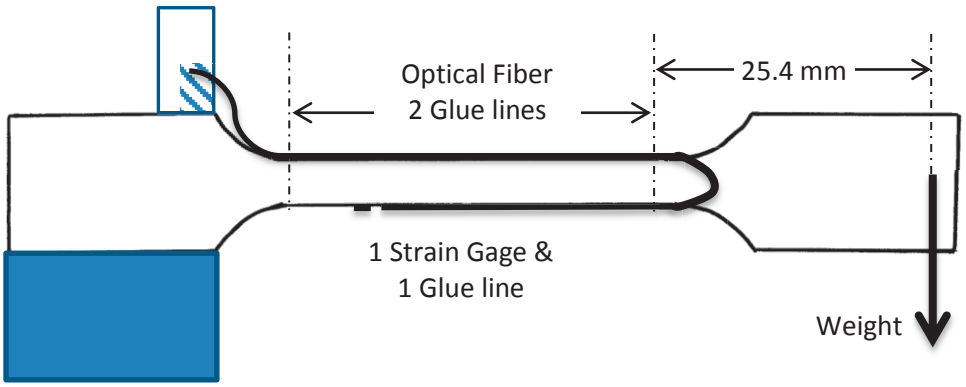

Figure 3.5 Cantilever beam loading of Specimen 3.2.

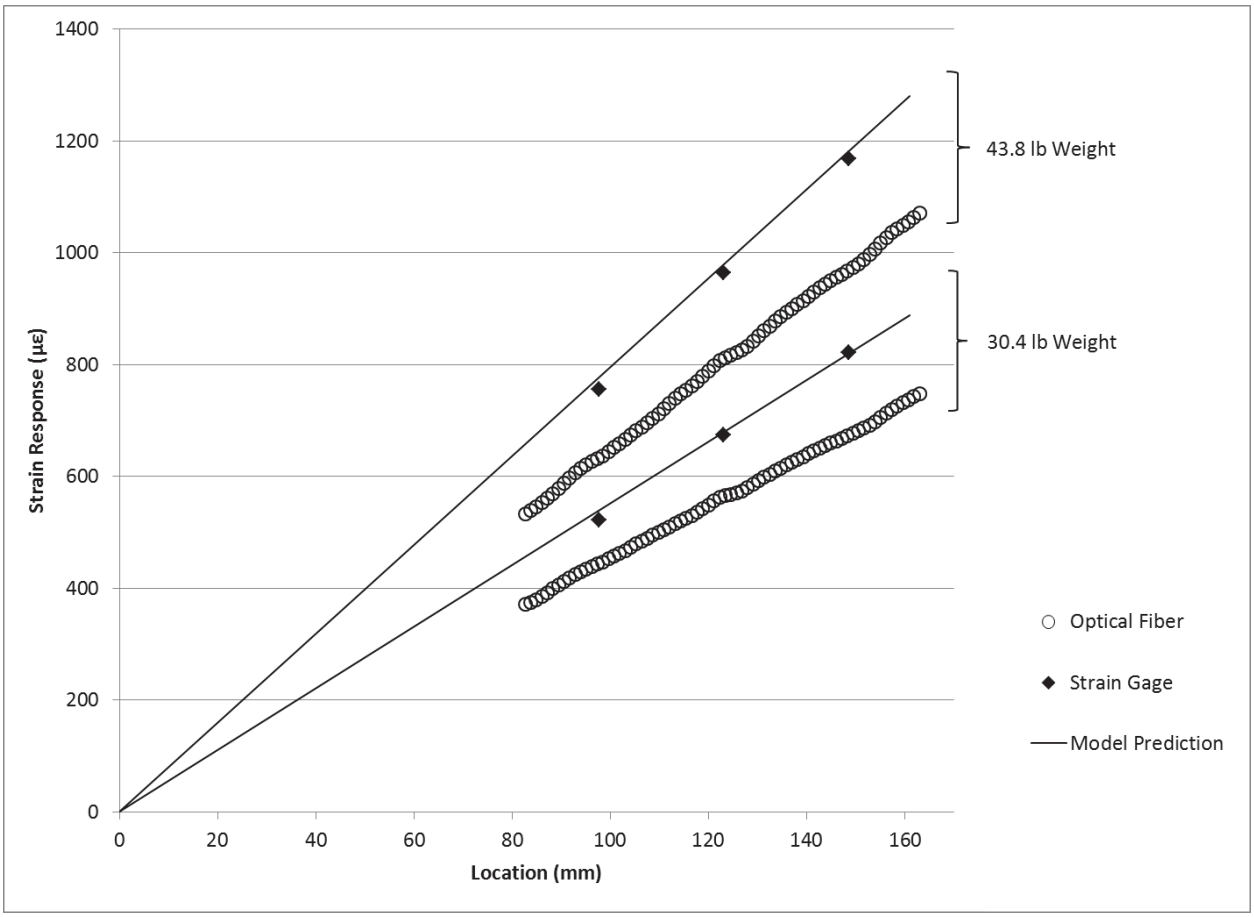

Figure 3.6 Results of a cantilever beam test on Specimen 3.1. Data from two different loads are shown. Note that the strain gage response matches the model predictions, but the response from the optical fiber strain sensors do not. The strain gage output was calibrated using a 100kΩ shunt resistor.

Also shown in the figure is the strain measured by each of the three conventional strain gages, as well as the linear strain gradients (solid lines) predicted by the strength of materials model for transverse loading of a beam for these two loads. Clearly, the conventional strain gages match the model predictions, and all data show a linear strain gradient, as expected. However, the strain outputs from the optical fiber sensors do not match that of the conventional strain gages or the model predictions. Therefore, an experimentally determined strain transfer factor was found in the following way:

$$\beta = \frac{Strain\ Gradient\ of\ Model}{Strain\ Gradient\ of\ Data}$$

The results of this calculation for both sets of data were averaged, and this produced a strain transfer factor of approximately β = 1.21. Then, the data from Figure 3.6 was multiplied by this factor and the result is shown in Figure 3.7.

Once this strain transfer factor was determined using the cantilever beam approach, the data collected in the axial test of Specimen 3.1 was adjusted accordingly. Some typical results of these axial tests are shown in Figure 3.8. This figure also shows the strain predicted by the following model equation for axial loading:

$$\varepsilon = \frac{P}{EA}$$

where P is the axial load (given by the load cell), E is the elastic modulus for the aluminum material, and A is the cross-sectional area of the specimen.

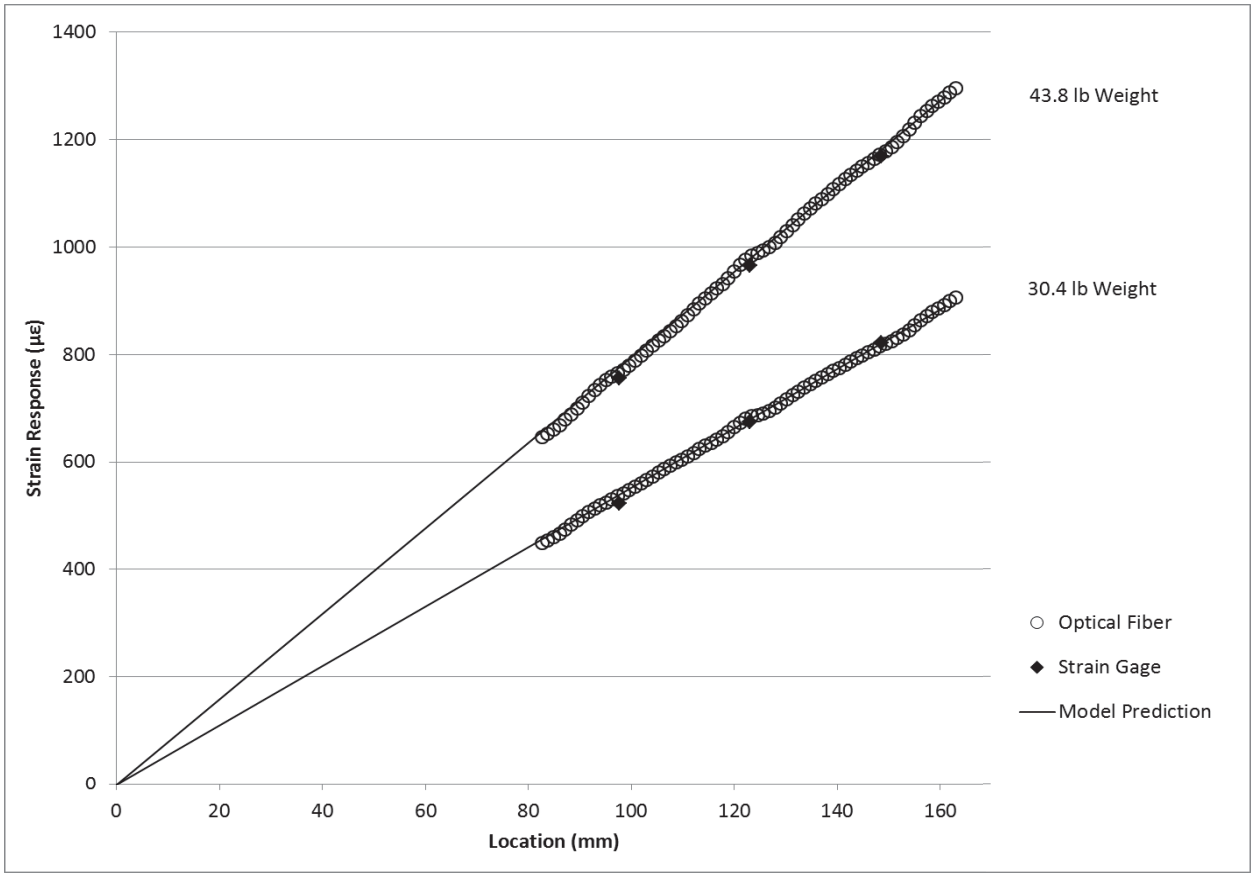

Figure 3.7 Data from Figure 3.6 with the optical fiber response multiplied by the strain transfer factor of 1.21.

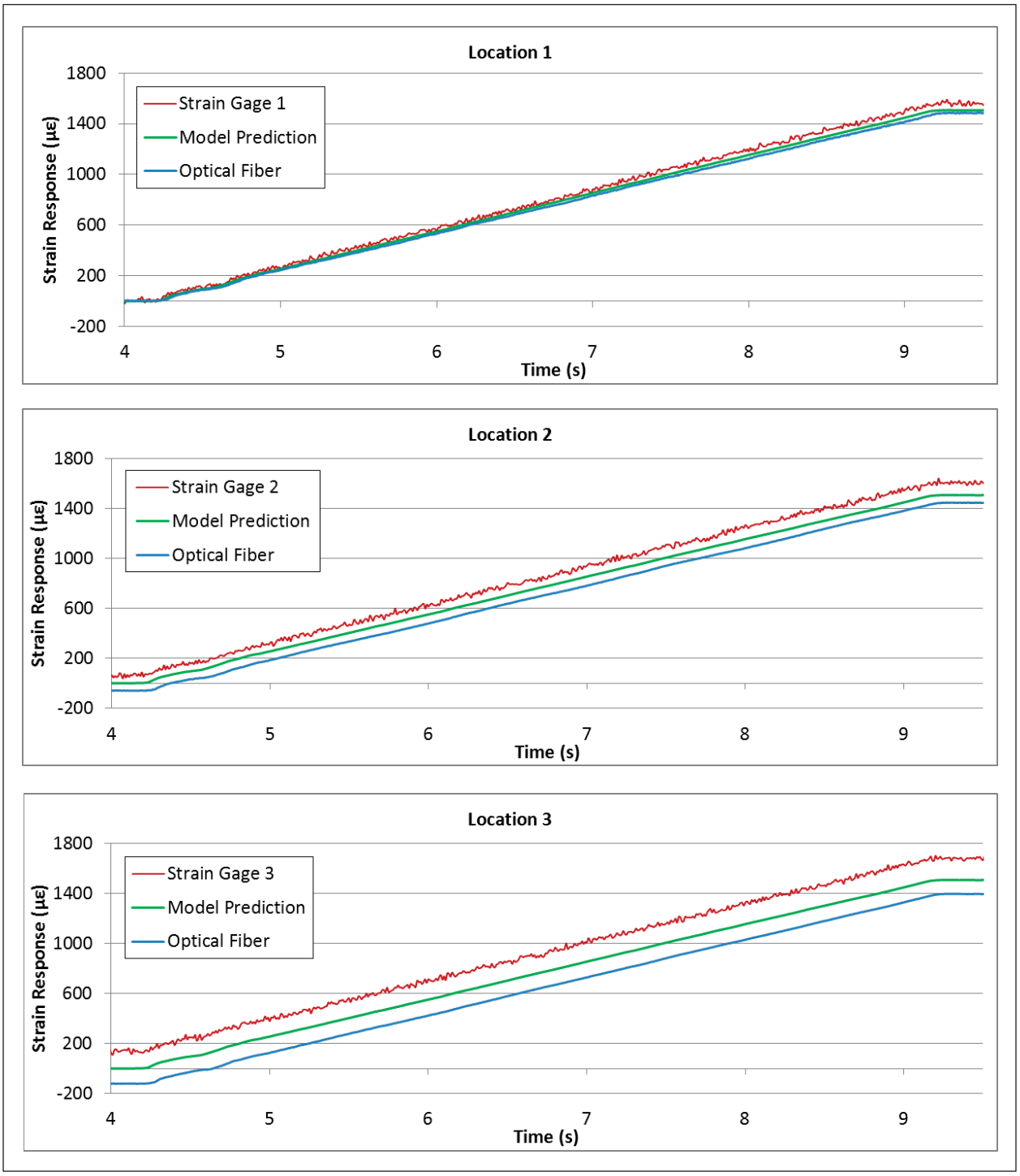

Figure 3.8 The strain response of the three conventional strain gages, collocated points in the optical fiber, and model predictions based on axial loading of Specimen 3.1. These points were spaced along the specimen on 25.4 mm (1 in) intervals. All data shown in this figure were collected simultaneously during the same test. The optical fiber strain data have been adjusted by the strain transfer factor of 1.21. Note that at each location, the strain response of the strain gage and that of the optical fiber (on the opposite side of the specimen) are symmetrical about the model prediction which only accounted for the case of pure axial loading.

What may not be clear in these graphs is that under this axial test, the specimen was apparently exposed to a linear strain gradient (which, of course, was not expected for an axial test). This gradient is shown in Figure 3.9. In this figure, the specimen was simply clamped, and the load cell indicated that the specimen was under no axial load. Clearly, the strain gage and optical fiber register approximately the same strain gradient magnitude of 2.5 με/mm. Once the specimen was loaded to a nominal axial strain of 1500 με (as determined by the load cell response), it was found that the strain gradients measured on each surface differed slightly more, with the optical fiber indicating approximately a 1.8 με/mm gradient, and the strain gages (on the opposite side) indicating approximately a 2.4 με/mm gradient (see Figure 3.10).

In order to investigate the effects that the three dimensional profile of a glue line might have on the strain transfer (and thus the strain response) of fiber optic strain sensors, a cantilever beam test was conducted on Specimen 3.2, using weights of 8.04 lb, 16.28 lb, 30.4 lb, and 43.8 lb. Since a similar test had been conducted on Specimen 3.1 (with a larger AE-10 glue line profile), Specimen 3.2 was manufactured with smaller and more uniform glue lines. Thus, using the AE-10 glue lines on Specimen 3.1 and Specimen 3.2, it was possible to compare the response of the two glue line profiles.

The second purpose of this test was to investigate the effects that different strain gage adhesives might have on this response. Since Specimen 3.2 was manufactured with both AE-10 and M-Bond 200 glue lines, a comparison between both adhesive types could be made.

The results of this test are shown in Figure 3.11. The data shown in this figure have been multiplied by the strain transfer factor ($\beta = 1.21$) determined from the cantilever beam test conducted on Specimen 3.1. The figure shows the results from three separate glue lines – two of which were one side of the specimen, and one of which was on the opposite side. The output from the one strain gage attached to this specimen is also shown, and the model predictions for these four loads are shown with a solid line.

In order to assess the variability observed in the strain transfer factor, a comparison was made by averaging those results for the cantilever beam test of Specimen 3.2 (with its three glue lines and two adhesive types). This was done by calculating and averaging the strain transfer factors for

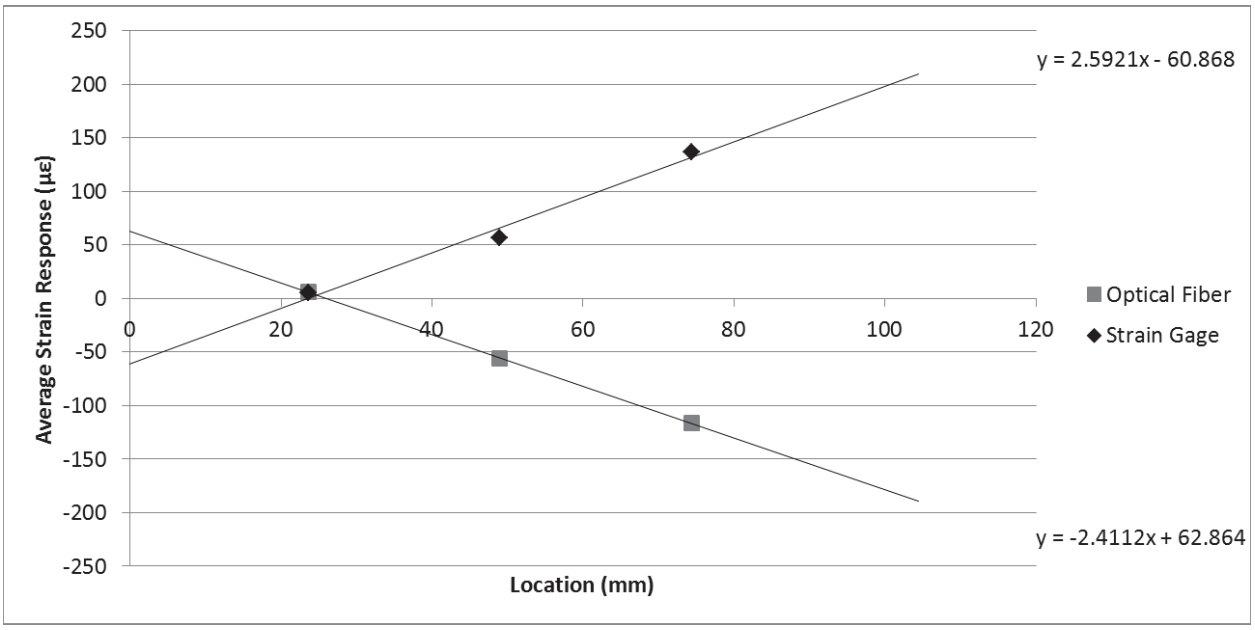

Figure 3.9 The strain gradient observed during axial testing of Specimen 3.1 by both the optical fiber strain sensors and the conventional strain gages. As these data were collected, the specimen was clamped in the hydraulic grips of the MTS 880 load frame and held at zero load in load control mode. The strain gradients observed were approximately equal in magnitude (~2.5 με/mm), but opposite in direction. The strain gages were on the opposite side of the specimen from the optical fiber.

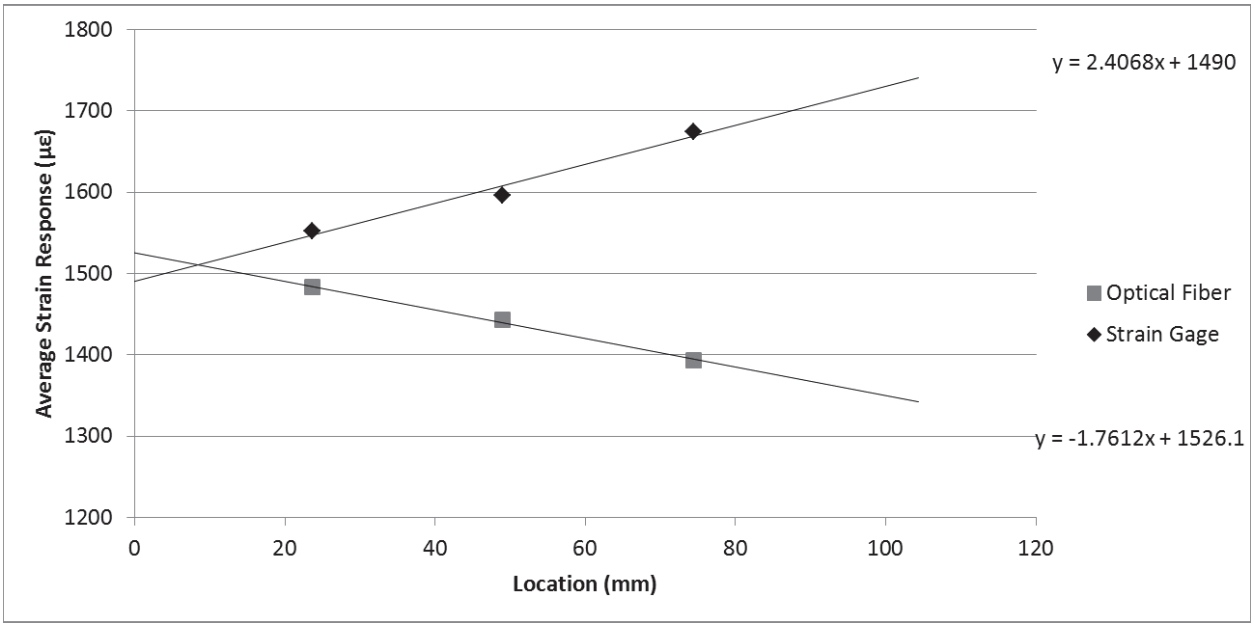

Figure 3.10 The strain gradient observed during axial testing of Specimen 3.1 by both the optical fiber strain sensors and the conventional strain gages. As these data were collected, the specimen was clamped in the hydraulic grips of the MTS 880 load frame and held at a load of 17.348 kN in load control mode (approximately 1500 με). The strain gradients observed differed slightly, with the strain gages showing a gradient of approximately 2.4 με/mm, and the optical fiber indicating a gradient of approximately -1.8 με/mm.

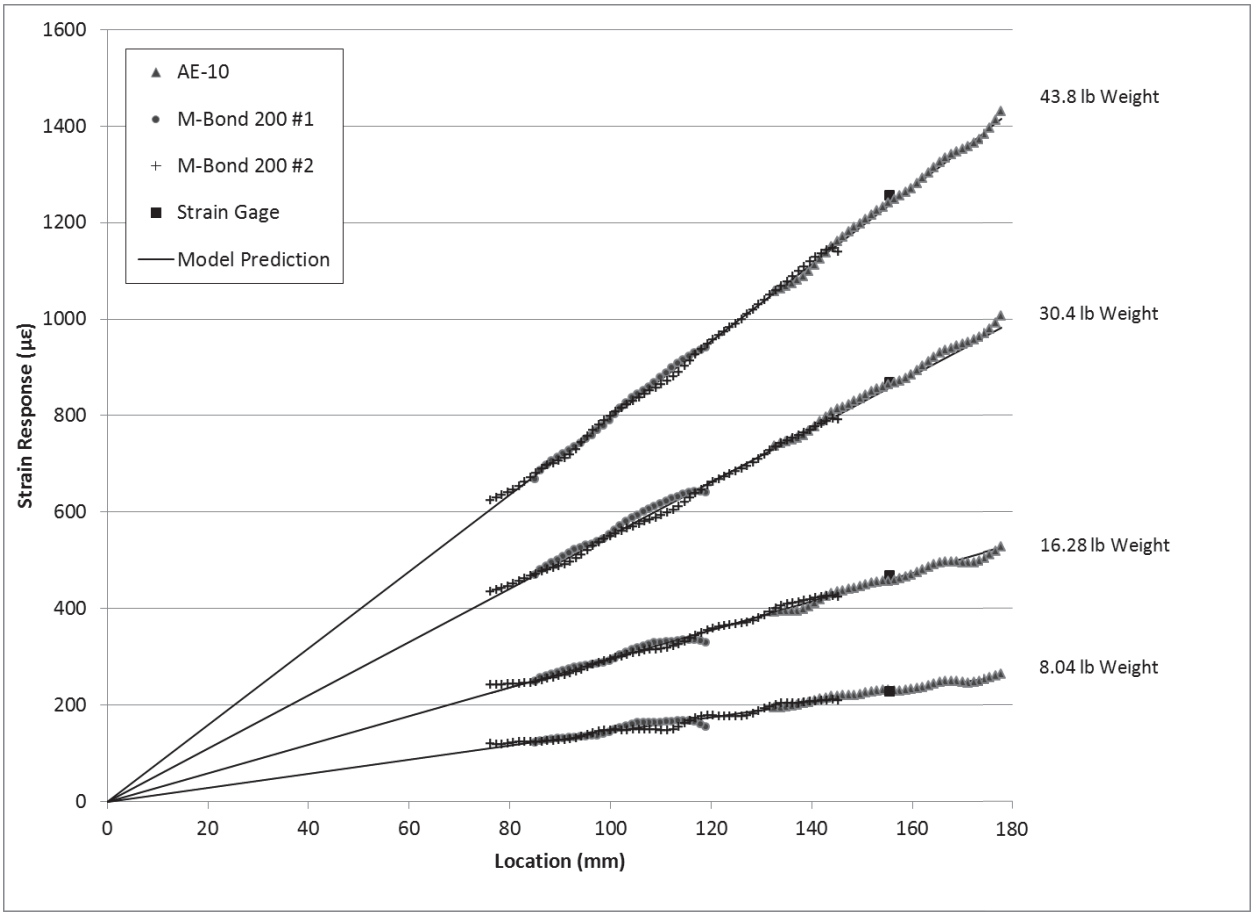

Figure 3.11 Results of cantilever beam testing of Specimen 3.2, using a strain transfer (multiplication) factor of 1.21 on the optical fiber strain data.

each of the four cantilever beam loads for each separate glue line. These averages are shown in Figure 3.12.

Finally, strain transfer results obtained from the polyimide coated optical fiber are shown in Figure 3.13. This figure shows the results from a steady ramp from no load to a tensile load of approximately 6500 lb applied to Specimen 3.3.

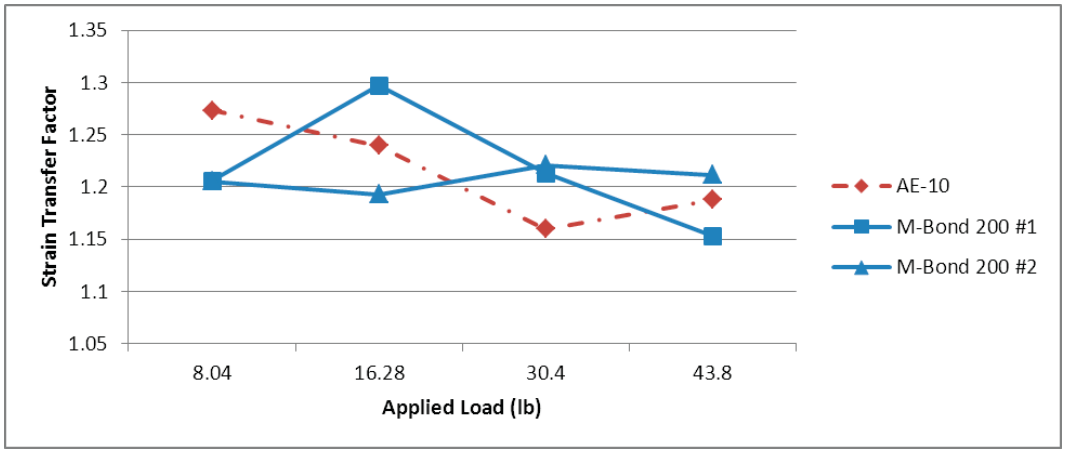

Figure 3.12 Strain transfer factors for three separate glue lines on Specimen 3.2 from cantilever beam testing using four different transverse loads. This shows that there is as much variability within a given type of adhesive as there is between the two different adhesive types used. All glue lines were applied using the same technique.

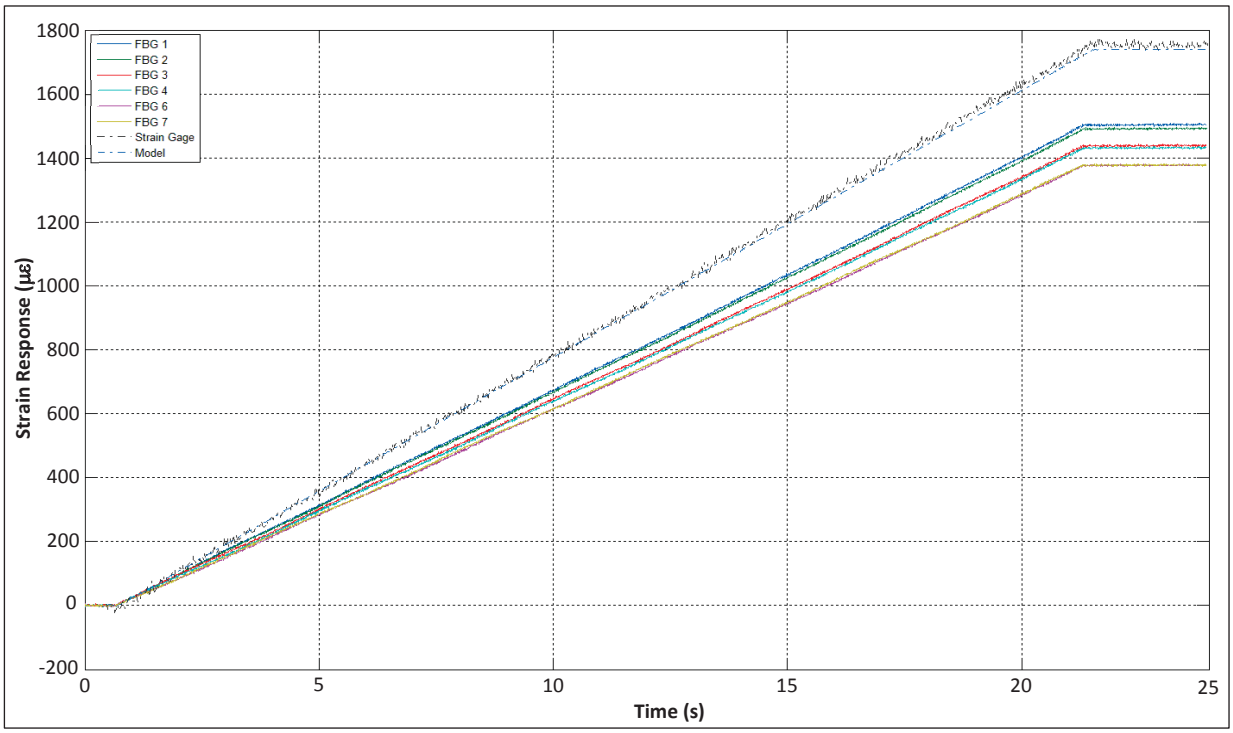

Figure 3.13 The strain response of 6 FBG sensors on Specimen 3.3 during a ramp from no load to a tensile load of approximately 6500 lb. The FBG response was compared to that of a conventional strain gage on the specimen and a model prediction based on the load cell response, the cross-sectional area, and the elastic modulus of the specimen.

3.4 Discussion

As can be seen in Figure 3.7, the model predictions and the strain gage data from the cantilever beam test overlap nearly perfectly, and the optical fiber data (modified by multiplying by the strain transfer factor of 1.21) match those predictions very well, too. The purpose of this test was specifically to determine the factor by which one must multiply the optical fiber strain data in order to make it match the known strain in the structure to which it is bonded. (Recall that this is thought to be due to the inability of the adhesive and fiber coating to transfer 100% of the applied strain because of their own elastic deformations.) Thus, this multiplier (1.21) was the objective of this cantilever beam test, and this value suggests that these combinations of adhesive and fiber coating are each capable of transferring approximately 82.6% of the actual strain at the attachment surface of the specimen.

In addition to finding the strain transfer factor, Figure 3.7 also demonstrates that the strain transfer factor is constant along the glue line. This is obvious because in the cantilever loading condition the strain is known to be a linear function of position with the slope being the strain gradient. Clearly, this figure shows this to be the case for the model predictions, for the conventional strain gage results, and (more importantly for this research) for the optical fiber results. Thus, the strain transfer factor of 1.21 does not vary with position in the glue line. Without such verification, it could not be assumed that this would be the case. Furthermore, it should be noted that this glue line was approximately 100 mm long and thus due to the observed linearity, this single glue line (by itself) provides data equivalent to that of several separate tests for a strain transfer factor. For instance, using just the first 10 mm of the glue line, one would arrive at a strain transfer factor of $\beta = 1.21$; however, due to this linearity, one would arrive at the same result using any 10 mm section of the glueline. Therefore, this single glue line provides a significant amount of data supporting the conclusion that the proper strain transfer factor for this combination of adhesive, optical fiber coating, and glue line profile is $\beta = 1.21$. The significance of this should not be overlooked.

Finally, these data indicate that the strain transfer factor is not dependent on the magnitude of applied strain. The reasoning behind this conclusion is, once again, the linearity of the optical fiber strain response. Note that, in this cantilever beam test, one end of the glue line was exposed

to a larger applied strain than the other (with a known linear variation in between), but a single strain transfer factor was sufficient to correct the strain response for the entire length of the glue line. Once again this could not be assumed without experimental verification, for this is essentially the linearity issue for which every sensing system must be analyzed.

Additional verification of the optical fiber strain response was obtained by considering the results of the axial tension test performed on Specimen 3.1. While at first glance, one might be concerned that the optical fiber response (shown in Figure 3.8) did not match that of the conventional strain gages, further investigation shows that the strain gage response did not match the model predictions (which were based on the calibrated load cell response and very well understood mechanics of materials). However, the strain response from points in the optical fiber which were at the same axial location as the three strain gages did respond in much the same way as the strain gages. For instance, as Figure 3.8 shows, at each location the optical fiber response and the strain gage response are basically symmetrical with respect to the model prediction. Since the optical fiber was located on the opposite side of the specimen from the strain gages, and since the model prediction was based solely on the load cell response (and thus did not account for any unknown bending moment in the beam), this behavior seems consistent. In fact, it appears that the hydraulic grips of the MTS testing machine were slightly misaligned because in Figure 3.8 and in Figure 3.9, it is obvious that the specimen was exposed to a strain gradient before any axial load was applied. Finally, the fact that the optical fiber response remains basically parallel to the model prediction (for each location considered) is evidence that the strain transfer factor of 1.21 determined in the cantilever beam test is the correct value for this combination of adhesive and fiber coating.

Since it is not obvious that different types of glue lines (due to different adhesives or to different geometries) will transfer strain equally, it was considered necessary to investigate whether or not different adhesives or glue profiles would alter the strain transfer capabilities. Therefore, Specimen 3.2 was constructed with both AE-10 and M-Bond 200 adhesives in such a way that the glue lines were smaller and more uniform. This made it possible to make the two necessary comparisons. First, the strain response for two distinctively different glue profiles (that of Specimen 3.1 and that of Specimen 3.2) were compared for a common type of adhesive (AE-10),

and then the strain response for distinctly different types of adhesives (AE-10 and M-Bond 200) with similar glue line profiles were compared. As can be seen in Figure 3.11, the strain response from each of the three glue lines on Specimen 3.2 match the model predictions quite well when corrected by the strain transfer factor determined by the analysis of Specimen 3.1. This indicates two things. First, the glue line profile does not have a significant effect on the strain response. In fact, it should be noted that the glue line on Specimen 3.1 did completely cover the optical fiber with a noticeable amount of glue. Others have noted a significant amount of birefringence if glue completely surrounds the fiber (Betz, 2003). However, this did not seem to have a detrimental effect on the strain response for the system used in this test. The second thing that can be observed from the results of this test is that both types of adhesives transferred strain equally well. Note that all of the optical fiber used in these tests (on Specimens 2.1 and 2.2) was coated in acrylate, so one should not assume that the strain transfer factor (of 1.21) found in these tests would apply to fibers with other coatings. Since it is widely considered that a polyimide coating transfers strain better than acrylate, one might expect it to be associated with a lower strain transfer factor.

Figure 3.12 shows that the strain transfer factors for the three separate glue lines on Specimen 3.2 do not show any particular trend with respect to applied strain, or with respect to adhesive type. This figure shows that the largest variation observed occurred within a single glue line which varied from as high as approximately 1.3 to as low as approximately 1.15. It is clear that there was as much variation in strain transfer within the two M-Bond 200 glue lines as there was between the AE-10 and either M-Bond 200 glue line.

Another conclusion that can be drawn from the results of Specimen 3.2 (as shown in Figure 3.11) is that the strain transfer factor of $\beta = 1.21$ is independent of whether the glue line is in compression or in tension. This conclusion is based on the observation that strain output from all three gluelines line up with the model predictions quite well even though one glue line was in compression while the other two were in tension.

Finally, it is necessary to compare the strain transfer results obtained from acrylate coated optical fiber (bonded with AE-10 and M-Bond 200) with those obtained from polyimide coated fiber (bonded with AE-15). Figure 3.13 shows the results of a steady ramp from no load to a tensile

load of approximately 6500 lb applied to Specimen 3.3. Just prior to this ramp, and with the specimen held in the grips at no load, a complete set of 24 second long baseline scans were taken from the strain gage, the load cell, and the optical fiber sensors. In post processing, these time series were averaged and subtracted from the subsequent test data as described above. Thus, it is no surprise that all of the sensors read zero at time t = 0. Notice that the conventional strain gage agrees with the model predictions nicely. This is not an artificial agreement. It means that the beam is behaving as predicted and that the conventional strain gage is returning the true strain, or that both are off by the same scale factor (which would be quite a coincidence). However, it appears that not all of the strain is being transferred through the adhesive to the optical fiber. This data also suggests that it may be appropriate to consider using a strain transfer factor to describe the fraction of true strain that is transferred. One such approach (for this sort of axial tension test) might be to define this coefficient according to the following:

$$\beta = \frac{Applied\ Strain}{Transferred\ Strain}$$

For this data (considering the seven discrete fiber Bragg grating strain sensors in the glue line), it was experimentally determined that the strain transfer factors were:

$B_1 = 1.151$

$B_2 = 1.174$

$B_3 = 1.215$

$B_4 = 1.215$

$B_6 = 1.259$

$B_7 = 1.266$

Due to complications related to using this system (designed for continuous grating fiber) to interrogate fiber with discrete Bragg gratings, the results for Sensor 5 were determined to be unreliable, and are not included in this discussion. However, since the remaining six FBG sensors were not affected, it should be sufficient to discuss the results of just those. Clearly, these strain transfer results are consistent with the result obtained from acrylate coated fiber. Specifically, these data (when averaged) yield a strain transfer factor of $\beta = 1.21$, which is

identical to that obtained earlier. Once again the variation observed from the different sensors, is due to a slight misalignment in the grips of the MTS testing machine. This project has shown that such an effect is typical.

3.5 Conclusions

The strain response of optical fibers was found to be consistently less than that of conventional strain gages and also less than that expected from model predictions. However, a strain transfer factor of 1.21 was found to be sufficient to correct the optical fiber strain response for both acrylate and polyimide coated fiber. This value suggests that these combinations of adhesive (M-Bond AE-10, M-Bond AE-15, and M-Bond 200) with acrylate and polyimide fiber coatings are capable of transmitting only about 82.6% of the actual strain in the specimen into the optical fiber core. It was found that this strain transfer effect was independent of the type of adhesive used, independent of the type of optical fiber coating used, and independent of the three-dimensional geometry of the glue line. It was further found that this strain transfer factor is sufficient for both tension and compression.

Chapter 4

Optical Fiber Sensing for Damage Detection in Composites

Abstract

A tension test was conducted on a composite specimen with a $[0, 90_3]_S$ layup to determine the feasibility of using optical fiber strain sensors for monitoring subcritical damage (such as matrix cracks) in fiber reinforced composite materials. These results indicate that the strain profile along one side of the specimen is approximately symmetric with respect to the strain profile along the opposite side. This suggests that, with an array of optical fibers which monitor the strain profile on both sides of a composite panel, it may be possible to predict the cross-sections where matrix cracks will form first and to monitor their severity.

4.1 Introduction

Fiber reinforced composite materials offer many advantages in engineering applications. However, these materials are susceptible to the formation of subcritical damage such as matrix cracks. So long as these flaws remain sufficiently small and do not intrude into more critical elements such as load bearing reinforcement fibers, they usually do not present a concern, especially if the composite is designed to accommodate them without failing. However, as with any internal damage, these matrix cracks serve as initiation points for more critical damage, especially under fatigue loading conditions. This additional damage includes such flaws as delamination of load bearing layers, transverse cracks in load bearing layers, and breakage of reinforcement fibers. Thus, it is sometimes useful to monitor the locations and severity of subcritical damage such as matrix cracks. The distributed sensing ability of optical fiber strain sensors may offer that capability. This technology may make it possible to better investigate the

mechanical response of fiber reinforced composite materials, to predict the formation of subcritical damage, and to monitor the progression of damage in the material. Therefore, the purpose of this test was to investigate the usefulness of optical fiber sensing for detecting subcritical damage in fiber reinforced composite materials.

4.2 Testing Methods

Specimen Design

In order to investigate the use of optical fibers for monitoring subcritical damage in composite materials, a specimen (Specimen 4.1) was constructed from a length of fiber reinforced, graphite-epoxy composite which was cut from a sheet of material. This material was manufactured at Virginia Tech with a $[0, 90_3]_S$ layup, and the specimen was cut such that the outside layers (the one layer on each surface, referred to as the "zero-plies") were oriented along the loading axis, and the six interior plies were oriented perpendicular to the loading axis. As cut, the specimen dimensions were 1 mm (0.04 in) thick by 12.7 mm (0.5 in) wide by approximately 300 mm (11.8 in) long. This specimen was instrumented with a single continuous-grating, acrylate-coated optical fiber which was bonded along one surface with AE-10 strain gage adhesive (applied by hand with a 22 gauge syringe) and along the opposite surface with M-Bond 200 (using a squeegee). This squeegee was simply a short length of ordinary automotive windshield blade. The application process was to simply tape the optical fiber in place (under slight tension), and then to place a drop of adhesive at one end of the desired glue line, and wipe it through smoothly to the other end using the squeegee. This technique produces a much smaller and more uniform glue line than does the syringe application. Furthermore, these glue lines are less likely to contain air bubbles in the adhesive which may be susceptible to fatigue damage and cause other strain anomalies. These glue lines are shown in Figure 4.1. This specimen did not have a conventional strain gage attached.

Testing Machines and Test Equipment

In order to interrogate the strain sensing optical fiber on this specimen, a High Speed Distributed Sensing System (HSDSS) on loan from the Blacksburg, VA facility of Luna Technologies was used. The particular system used in this testing was a DSS 8600B, and contained features and capabilities which were, at the time, still under development. This system was designed to

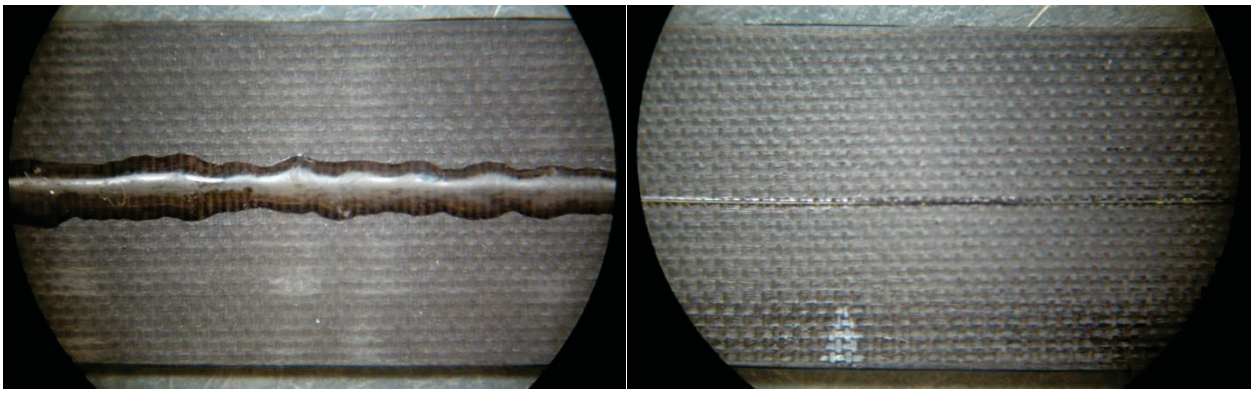

Figure 4.1 Close up of the two glue lines of Specimen 4.1 at the same magnification. The optical fiber was bonded for strain measurements using a 22 gauge blunted syringe with AE-10 adhesive on one side (left photo), and using the squeegee technique with M-Bond 200 on the other (right photo). The width of the composite specimen (vertical in these photos) was 0.5 in.

interrogate optical fiber containing a continuous Bragg grating, and was capable of returning individual strain readings from along the sensing fiber with a spatial resolution of approximately 0.0899 mm. This system was capable of scanning and collecting data at several hundred Hertz. However, in this test, data was collected at 200 Hz. The software used to operate the HSDSS (also on loan from Luna Innovations) was DSS 8600 v0.3 beta. Specimen 4.1 was tested in tension using an Instron 1125 screw-operated mechanical test stand (with a 20 kip load cell) which was not computer controlled.

Testing Procedures

The specimen was subjected to a simple tension test by mounting it in an Instron test stand and loading it at a constant cross-head rate of 0.5 mm/min until the observed strain exceeded 3000 με. In order to reduce the effect of misalignment in the grips, the testing machine was equipped with an upper grip which permitted the grip to swivel on a universal joint. The lower grip was fixed and did not swivel.

4.3 Results

Once the strain transfer factor was determined from the cantilever beam results, and verification was made that this factor did not vary much with adhesive type or glue line profile (as described in Chapter 3), a tension test was conducted on Specimen 4.1 in order to investigate the suitability of using optical fiber sensors to monitor subcritical damage in a fiber reinforced composite panel. As described earlier, two different glue line profiles and two types of adhesives were used in instrumenting this specimen.

The strain distribution was found to vary considerably along both sides of the specimen (see Figure 4.2). This data has been smoothed using a 5-point moving average in the spatial direction (not in time), and has been multiplied by a strain transfer factor of 1.21. This figure shows three typical strain profiles (collected from collocated points along both sides of the specimen) for nominal strains of approximately 1000, 2000, and 3000 με. Since these strain profiles show obvious symmetry between the strain profile of one side and that of the other, the point-wise difference between the strain measured on side one (bonded with AE-10) and that measured on side two (bonded with M-Bond 200) was calculated. These strain difference profiles are also shown in the figure. These curves and this symmetry are typical of the data collected for this test, with only the strain magnitudes varying with increasing load. Note that the data in this figure are plotted versus location on the specimen, with 0 mm being located near the end of the glue line which was nearest the rigid lower grip of the Instron.

In order to better understand the strain response measured on both sides of the specimen, the strain difference (computed as described above) for various locations along the specimen was plotted versus time. Since during this time the specimen was exposed to linearly increasing strain (due to the constant cross-head displacement rate), the curves produced are qualitatively the same as would be seen by plotting this strain difference versus applied load or versus nominal strain. Figure 4.3 shows these curves for four typical locations: 9.1, 26.0, 28.3, and 60.0 mm. These particular locations were chosen because these curves reveal the various qualitatively different behaviors observed.

4.4 Discussion

The data presented in this chapter have been increased by a factor of 1.21 which is the strain transfer factor determined for this combination of fiber coating and strain gage adhesives in earlier tests (refer to Chapter 3). This was done for the optical fiber strain data from this composite material without reference to either a conventional strain gage measurement or a theoretical strain based the load cell response. The reason for this is based on the observation that the adhesive remained bonded to the composite specimen at all times, and that there is no theoretical way that the mechanical behavior (which determines the strain transfer capability) of the glue line can depend on the composition of material to which it is bonded – so long as no debonding takes place.

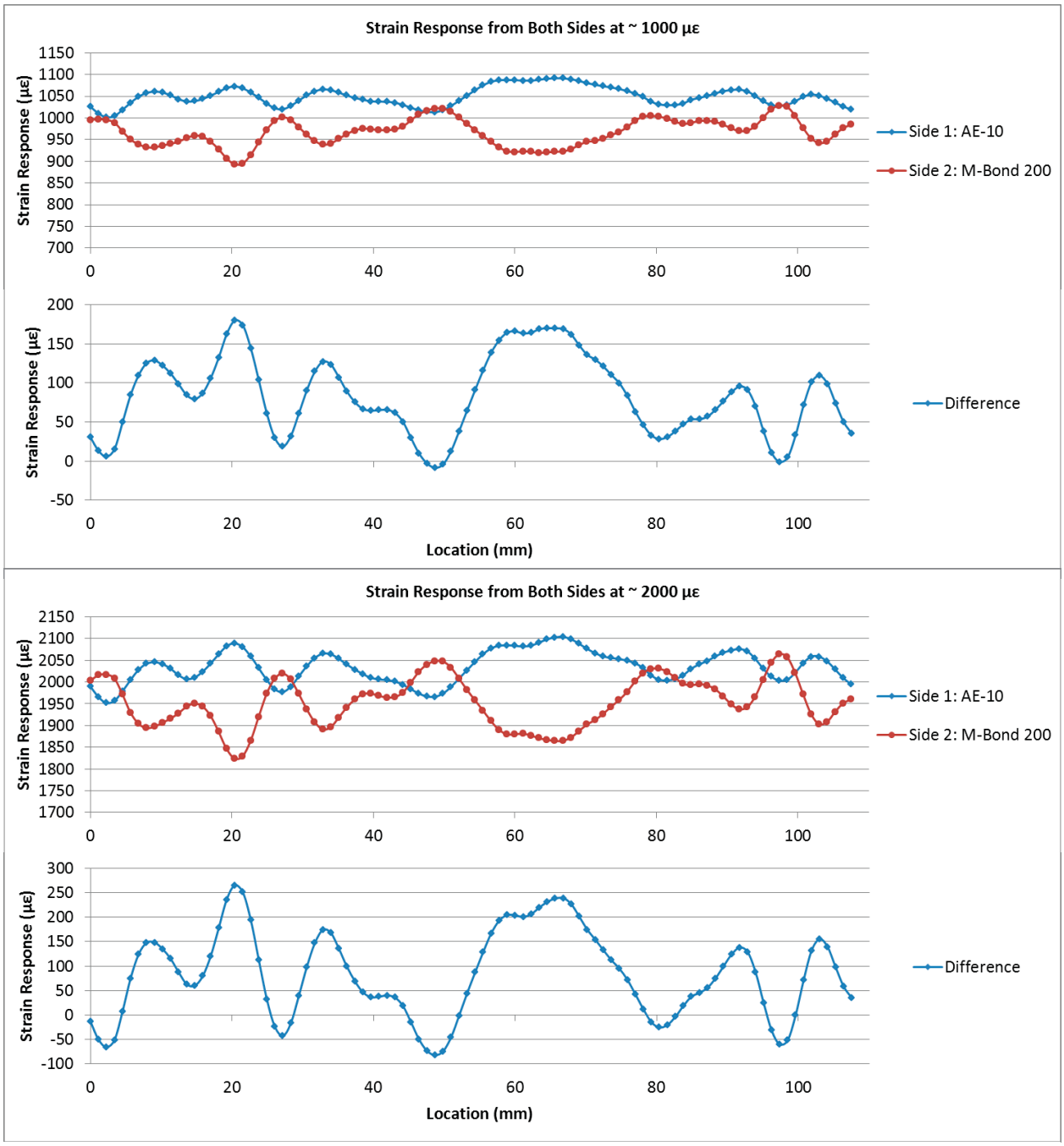

Figure 4.2 Typical strain distribution on both sides of Specimen 4.1. This composite specimen was instrumented with a single optical fiber which was bonded to side one with AE-10 (applied with 22 gauge syringe), and wrapped around to side two, where it was attached with M-Bond 200 (applied with squeegee). This figure shows the strain response for both glue lines for nominal strains of 1000, 2000, and 3000 με (next page). For each, the upper plot is the strain distribution and the lower plot is the difference between the strain measured on side one (AE-10) minus that measured on side two (M-Bond 200). (Continued)

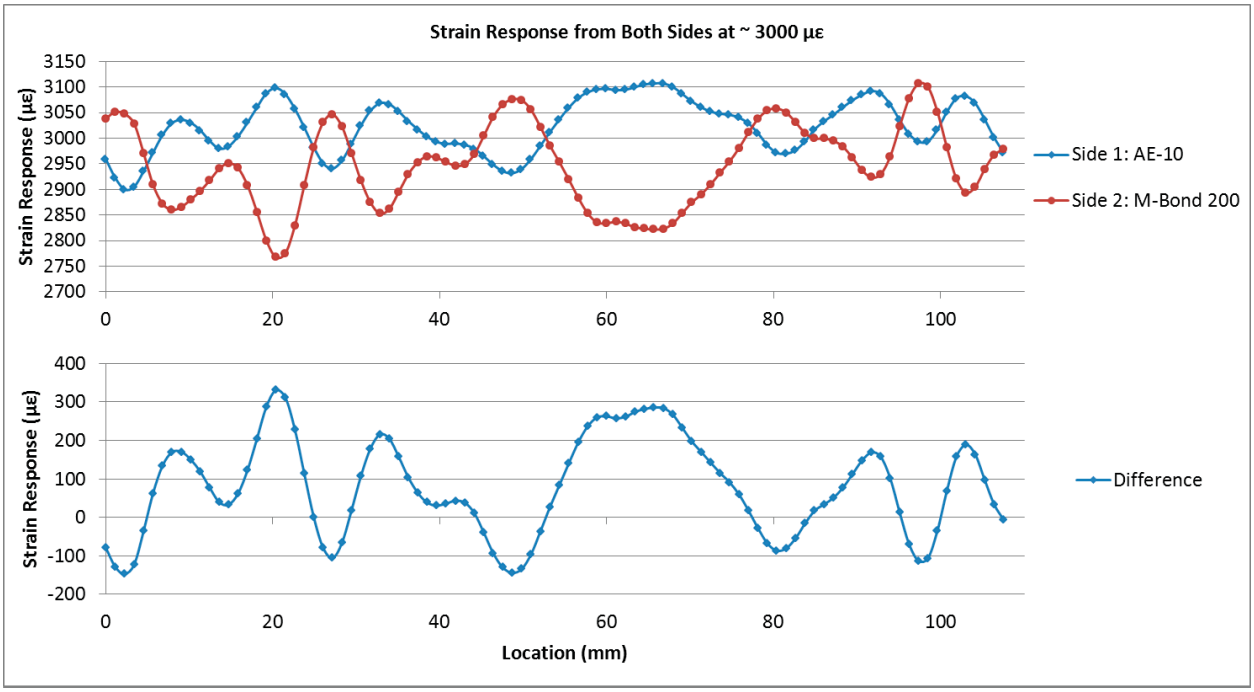

Figure 4.2 (Continued from previous page). Note the symmetry between the strain distribution on side one and that of side two. This symmetry was found to develop at low strain levels (being obvious by 1000 με) and to persist with increasing strain.

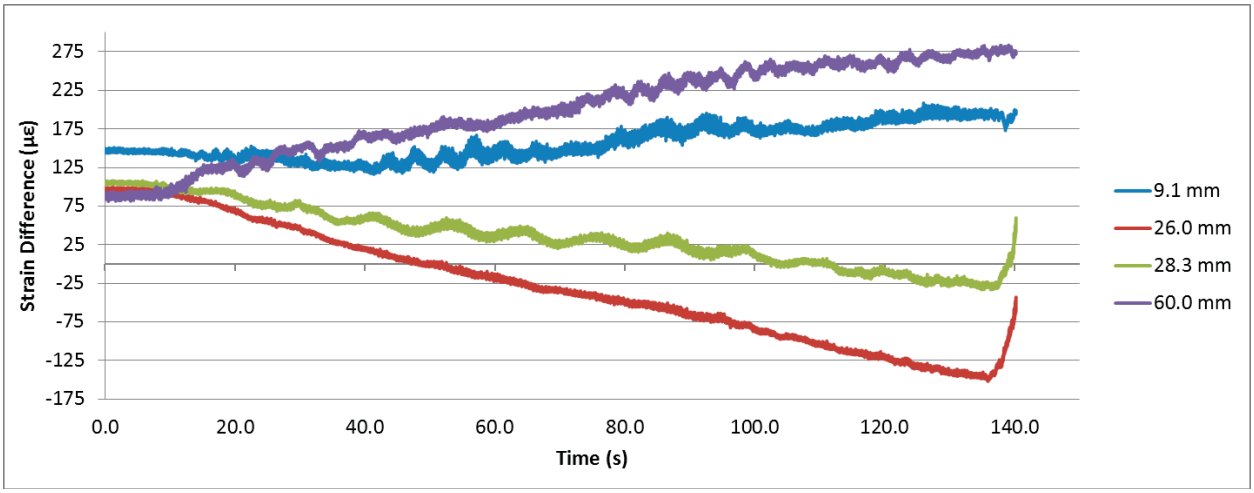

Figure 4.3 The difference between the strain measured on side one (AE-10) minus that measured on side two (M-Bond 200) plotted versus time (for four representative cross-sections of Specimen 4.1). Since the specimen was loaded axially at a constant cross-head displacement rate, these curves are qualitatively the same as would be obtained by plotting versus applied load or nominal strain. Note that different cross-sections responded somewhat differently to increasing nominal strain – some with a regular transfer of strain from one side of the cross-section to the other, and others with regular or irregular oscillation about such a trend.

Given the degree of variation in strain (see Figure 4.2) from various points in the optical fiber (especially when attached to a composite panel), one may not be able to use a single optical fiber glue line for locating subcritical damage on the small scale of matrix cracks. However, these tests indicate that it may still be possible to monitor such small effects using an array of fibers which monitor the strain distribution on both sides of the composite panel. As Figure 4.2 shows, in this test the strain profile from one side of the composite panel was quite symmetrical with respect to the strain profile from the other side. This suggests that the stiffness of the specimen varied through each cross-section. In other words, since in most cross-sections the strain on one side of the specimen did not equal that on the other side, it appears that the specimen was generally stiffer on one side than the other. However, it should be noted that this effect was not constant along the length of the specimen. For instance, in some cross-sections, one side exhibited more strain than the other, while other cross-sections exhibited the opposite effect.

One potential explanation for the presence of such large variations in the strain profile might be the existence of matrix cracks in the specimen. However, once the test was complete, the specimen was carefully checked for matrix cracks along both edges using a compound optical microscope, and it was found that none were present.

The likely explanation for this is that the composite panel had some natural variation in mechanical properties through both its length and its thickness. Thus, as the specimen was loaded axially, originally plane cross-sections did not remain plane. This suggests that strain measurements taken from embedded optical fibers should not be expected to register the same strain as a strain gage that is mounted on the surface directly above the fiber. Thus, such disagreement does not necessarily indicate an error in either measurement, but should be interpreted as evidence of a non-uniform strain distribution through that cross-section. This is a significant point which should not be overlooked. The conventional approach to solid mechanics which assumes that plane cross-sections remain plane under axial deformation clearly does not apply to non-homogeneous, non-isotropic composite materials.

The nominal strain in any given cross-section should be approximately the average of that measured on both sides for that cross-section. Furthermore, one might expect that regions where one side of the panel exhibits significantly more strain (such as around the 20 and 65 mm marks in Figure 4.2) to be ideal locations for the origination of matrix cracks or other subcritical

damage. Furthermore, once a crack is fully developed, one should expect to see a noticeable change of character in the symmetry or strain difference profile around that location. These effects may lead to the ability to predict the location of matrix cracks and the ability to monitor their growth in the specimen.

Figure 4.3 also demonstrates some interesting behavior for this specimen. This data is the difference between the strain measured on one surface and that measured at collocated points on the opposite surface (at the four given locations in the glue line). These curves suggest that the different cross-sections of the composite specimen responded somewhat differently as additional load was applied. For instance, the cross-section located at 26.0 mm originally exhibited more strain on one side, but as nominal strain increased, it regularly transferred strain to the opposite side. However, the cross-section at 28.3 mm, which also exhibited the same overall trend, oscillated regularly about that trend. The "hook" at the end of these two curves is of special interest, but until further investigation can be done, an explanation is lacking. The remaining two cross-sections shown (at 9.1 and 60.0 mm) shifted strain in the opposite direction with less regular or predictable oscillations. A good explanation for these behaviors requires additional study, but may shed additional light on the mechanical response of composite materials.

4.5 Conclusions

These results suggest that strain may vary by as much as several hundred microstrain along a length of fiber reinforced composite. Thus, it may not be possible to monitor subcritical damage in these materials using a single optical fiber attached to one side of a specimen, because the single optical fiber may not be resolve the minute strain gradients associated with matrix cracks from the natural strain variations due to inhomogeneities in the material and to random variation in the material stiffness.

However, these results indicate that by using an array of fibers to monitor the strain distribution on both sides of a composite panel, it may be possible to predict where subcritical damage is most likely to occur and to monitor the progression of such damage. This is due to the symmetry observed in the strain profile present on one surface of the composite with respect to that on the other surface. Furthermore, in the case of a composite panel which is fully populated with matrix cracks, further signal analysis (such as an FFT) of the distributed optical fiber strain data may show a frequency component which is associated with the regular spacing of these cracks.

Chapter 5

Summary and Conclusions

Mechanical fatigue testing of optical fiber Bragg grating strain sensors bonded to 7075-T651 aluminum with M-Bond AE-10 strain gage adhesive has been conducted. For strain amplitudes less than +/- 3000 με, these results do not indicate that the strain sensors or the glue line were compromised due to mechanical fatigue. These sensors were each performing to expectations just prior to the failure of the aluminum specimen itself, and a visual examination of the glue line did not reveal any debonding of the optical fiber. Each of the sensors monitored in this fatigue test returned strain values which were within a few dozen microstrain of that expected for the expected loading conditions, and these strain signals contained relatively low noise. Once the thermal strain was accounted for in these signals, the standard deviation was less than 3 με, which is far less than that of a conventional strain gage system.

However, for strain amplitudes as high as +/- 3500 με, these fatigue test results show that some fatigue damage may have occurred. While the adhesive bond itself did not fail (in that no debonding was observed), three of the sixteen strain sensors monitored did fail to respond as expected based on earlier results and on the response of adjacent sensors. The response of these sensors did appear to get worse with increasing fatigue, with the worst condition occurring just prior to specimen failure. At that point, one sensor recorded strain levels in tension which were almost 2000 με below the expected value.

When optical fiber strain sensors (both discrete Bragg gratings and continuous gratings) were interrogated with the High Speed Distributed Sensing System (HSDSS), the strain response of

these fiber sensors was found to be consistently less than that of conventional strain gages and also less than that expected from model predictions. However, a strain transfer factor of 1.21 was found to be sufficient to correct the optical fiber strain response for both polyimide coated and acrylate coated fibers. This value suggests that these combinations of adhesive (M-Bond AE-10, M-Bond AE-15, and M-Bond 200) and acrylate fiber coating are capable of transmitting only about 82.6% of the actual strain in the specimen into the optical fiber core. It was found that this strain transfer effect was independent of the type of adhesive used and independent of the three-dimensional geometry of the glue line. Additional results show that this strain transfer factor does not depend significantly on whether the fiber is coated in acrylate or in polyimide because both require the same strain transfer factor.

However, it is worth noting that the strain response of the Distributed Sensing System (DSS) used in the durability tests discussed in Chapter 2 was consistent with the nominal strain expected based on the axial load applied. These durability tests were conducted on the same type of specimen, using the same type of adhesive, and the same polyimide coating as the later strain transfer tests discussed in Chapter 3. The only notable difference was the strain measurement system used to interrogate the sensors. This suggests that perhaps the DSS system (used in the durability testing) was programmed to account for strain transfer issues, whereas the HSDSS system (used in the strain transfer testing) was not.

Additional testing which investigates the reliability of the strain transfer factor under fatigue loading conditions should also be conducted. For instance, a fatigue test which exposes optical fiber strain sensors to mechanical fatigue such as that described in Chapter 2, should be combined with the strain transfer testing discussed in Chapter 3. In such a test, the strain returned by the optical fiber sensors should be compared to the known strain by periodically halting the fatigue test, and performing a cantilever beam test with known weights. In this way, the optical fiber strain results could be verified in a way that cannot be done in a conventional fatigue test.

Finally, a test was conducted to investigate the plausibility of using optical fiber distributed strain sensing to predict and monitor subcritical damage in composite materials. These results suggest that due to the magnitude of the natural strain variation along the optical fiber (when bonded to composite materials), this technique may not be sufficient to detect the minute strain gradients associated with matrix cracks in composite materials using a single optical fiber glue

line. However, in the case of a composite panel which is fully populated with matrix cracks, further signal analysis (such as an FFT) of the distributed optical fiber strain data may show a frequency component which is associated with the regular spacing of these cracks. Furthermore, these results indicate that by using an array of fibers to monitor the strain distribution on both sides of a composite panel, it may be possible to predict where subcritical damage is most likely to occur and to monitor the progression of such damage. This theory is based on the observation (discussed in Chapter 4) that the strain profile along one surface of the composite specimen tested in this project was quite symmetric with respect to the strain profile along the other surface. This suggests that the mechanical properties of the fiber reinforced plies from which the composite was constructed varied from place to place. This inhomogeneity caused strain to be transferred from one surface to the other, and this produced regions in the underlying matrix where the strain was significantly higher nearer one surface than the other. This suggests that such locations are the best candidates for matrix crack formation.

References

Betz, Daniel C., Lothar Staudigel, Michael N. Trutzel, and Michael Kehlenbach, “Structural Monitoring Using Fiber-Optic Bragg Grating Sensors,” Structural Health Monitoring 2, no. 2 (June 2003): 145-152.

Erdogan, Turan, “Fiber grating spectra,” Journal of Lightwave Technology 15, no. 8 (August 1997): 1277-1294.

Güemes, Alfredo, Antonio Fernández-López, and Brian Soller, “Optical fiber distributed sensing - Physical principles and applications,” Structural Health Monitoring (May 2010): 233-245.

Gifford, Dawn K., Daniel R. Metrey, Mark E. Froggatt, Martin E. Rogers, and Alex K. Sang, “Monitoring strain during composite manufacturing using embedded distributed optical fiber sensing,” Paper presented at the SAMPE 2011 State of the Industry: Advanced Materials, Applications, and Processing Technology Conference (May 2011).

Habel, Wolfgang R., "Standards and guidelines: Could they enhance user confidence in fiber sensor technology?". Proc. SPIE 6619, 661906 (2007).

Hill, Kenneth, and Gerald Meltz, “Fiber Bragg grating technology fundamentals and overview.” Journal of Lightwave Technology 15, no. 8 (August 1997): 1263-1276.

Kersey, Alan D, “A review of recent developments in fiber optic sensor technology,” Optical Fiber Technology 2, no. 3 (1996): 291-317.

Kersey, Alan D., M.A. Davis, H.J. Patrick, M. LeBlanc, K.P. Koo, C.G. Askins, M.A. Putnam, and E.J. Friebele, “Fiber grating sensors,” Journal of Lightwave Technology 15, no. 8 (August 1997): 1442-1463.

Li, Dong-Sheng, and Hong-Nan Li, "Strain transferring of embedded fiber Bragg grating sensors", Proc. SPIE 5765, 1085 (2005).

Peairs, Daniel, Lisa Sterner, Kevin Flanagan, and Vladimir Kochergin, “Fiber optic monitoring of structural composites using optical backscatter reflectometry,” Society for the Advancement of Material and Process Engineering (2009).

Zhou, Guang-dong, Hong-nan Li, Liang Ren and Dong-sheng Li, "Influencing parameters analysis of strain transfer in optic fiber Bragg grating sensors", Proc. SPIE 6179, 61790R (2006).